Lyle, M., Wilson, P.A., Janecek, T.R., et al., 2002
Proceedings of the Ocean Drilling Program, Initial Reports Volume 199

9. Site 1216[1]

Shipboard Scientific Party[2]

BACKGROUND AND OBJECTIVES

Site 1216 (21°27.16′N, 139°28.79′W; 5152 meters below sea level [mbsl]; Fig. F1) is situated in abyssal hill topography south of the Molokai Fracture Zone and two small associated unnamed parasitic fracture zones (Fig. F2). Based on magnetic lineations, Site 1216 appears to be situated on normal ocean crust formed during the C25r magnetic anomaly (~57 Ma; Atwater and Severinghaus, 1989). Site 1216 was chosen for drilling because it is near the thickest section of lower Eocene sediments along the 56-Ma transect, which was based upon the seismic stratigraphy of seismic reflection data acquired on site survey cruise EW9709 during transits between the proposed drill sites (**Lyle et al.,** this volume; Moore et al., 2002). The Cenozoic history of sedimentation in this region was poorly constrained prior to Leg 199, being largely based on two Deep Sea Drilling Project (DSDP) drill sites (40 and 41) and piston core data (EW9709-3PC) from ~1.5° in latitude to the south. Based on data from these drill sites, we expected the sedimentary sequence at Site 1216 to comprise red clays (a mixture of wind-blown dust and authigenic precipitates) overlying a biogenic sediment section composed of an upper middle Eocene radiolarian ooze and lower carbonate ooze deposited when the site was near the ridge crest in the late Paleocene and early Eocene.

The broad paleoceanographic objectives of drilling the sedimentary sequence anticipated at Site 1216 are as follows: (1) to help define the shift in the Intertropical Convergence Zone through the Paleogene by following the change in eolian-dust composition and flux through time (red clays) and (2) to help define the latitudinal extent, composition, and mass accumulation of plankton communities in the north equatorial Pacific region thereby constraining ocean circulation patterns and the extent of the equatorial high-productivity belt in the Eocene ocean.

F1. Site location map, p. 16.

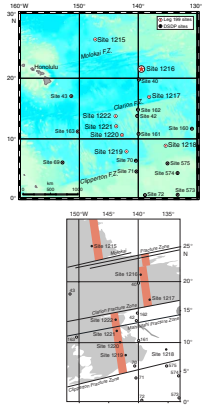

F2. Seismic reflection profile, p. 17.

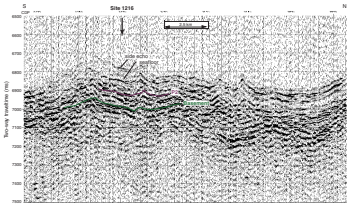

[1]**Examples of how to reference the whole or part of this volume.**
[2]**Shipboard Scientific Party addresses.**

Ms 199IR-109

Results from Site 1216 will also provide important information to test whether there was significant motion of the Hawaiian hotspot with respect to the Earth's spin axis during the early Cenozoic. At 56 Ma, the backtracked location of Site 1216 based upon a hotspot reference frame (Gripp and Gordon, 1990, for 0- to 5-Ma Pacific hotspot rotation pole; Engebretson et al., 1985, for older poles) is about 9°N, 108°W. If significant hotspot motion or true polar wander occurred since 57 Ma (Petronotis et al., 1994), this drill site could have been much nearer to the equator.

SUMMARY

Site 1216 (21°27.16′N, 139°28.79′W) is located on abyssal hills just south of the Molokai Fracture Zone at a water depth of 5163 m. The crustal age based on magnetic lineations is ~57 Ma (magnetic Anomaly An25r). The site was chosen for drilling because it is near the thickest section of lower Eocene sediments along the 56-Ma transect. Based on previous coring and drilling ~1° in latitude to the south, we expected to find a moderately thin red-clay section overlying middle Eocene radiolarian oozes and lower Eocene carbonates. Instead, we drilled a 50-m section of red clay overlying thin cherts in sediment and abandoned the site before reaching basement. We recovered only chert in the chert–sediment section. Microfossils are absent until ~40 meters below seafloor (mbsf), where small numbers of middle Eocene radiolarians appear. The cherts are early middle Eocene–early Eocene in age. We abandoned the site after drilling to 62 mbsf because of the likelihood of large amounts of chert in the section with little sediment recovery and because we could use the saved time to ensure more complete programs at the remaining sites.

The red-clay unit is similar to the red-clay section of Site 1215 but expanded (40 m vs. 25 m thick). The upper part of Site 1216 red clays are illite rich (based upon light absorption spectroscopy [LAS]), grading to smectite rich at the base. The transition begins at ~10 mbsf. Fe-Mn oxyhydroxides are also abundant in the lower part of the red clays, reaching a maximum of ~29 mbsf, as shown by bulk-sediment analyses and grain density. A transition from relatively high to low natural gamma ray (NGR) activity occurred at ~25 mbsf. A similar transition in NGR activity was observed at Site 1215.

The sediments at Site 1216 are surprisingly barren of microfossils. Upper–middle Eocene radiolarian oozes are absent at the site, and lower–middle Eocene radiolarians are not abundant. Calcareous microfossils are absent in the drilled section. Only agglutinated benthic foraminifers were found, but none are age diagnostic. The uppermost radiolarians (from Zone RP13; ~44 Ma) occur at ~40 mbsf. The base of the drilled section (62.2 mbsf) is in radiolarian Zones RP9 and RP10, which straddle the middle/early Eocene boundary (~49 Ma). The first cherts encountered downhole occurred at ~50 mbsf. Thus, these upper cherts appear in an interval of slow sedimentation rates, at most 4–5 m/m.y., presumably at the top of more rapidly deposited, lower Eocene sediments with larger amounts of biogenic components. We estimated from the seismic reflection profile that ~60 m of sediments remained to be drilled within the cherty section until basement was reached.

It was possible to identify magnetic polarity chrons in the red-clay section but none in sections with microfossils because of coring disturbance. Based on the microfossil dates, the oldest chron detected is prob-

ably C20n. Magnetic intensity of the red clays is strong, and drilling-induced magnetic overprints are mostly removable by standard procedures.

Highlights

Red-Clay Section

The red-clay section at Site 1216 has several similarities to the red-clay section cored at Site 1215, although it is 165% thicker. Both red-clay units have a transition from illite to smectite with depth. Both show a significant decrease in NGR activity downcore. The lower parts of each red-clay unit are enriched in Fe-Mn oxyhydroxides. When multisensor track (MST) records are compared, smaller events appear to correlate between these two sites. Provided that some age control can be developed, it may prove possible to develop a much more detailed red-clay stratigraphy for the North Pacific than is now available.

Missing Middle Eocene Radiolarian Oozes

One of the major surprises found from drilling Site 1216 is the remarkable lack of late or middle Eocene radiolarian oozes. These are biogenic sediments that have no modern analog but are prominent sedimentary features from piston cores and drill sites only 1° to the south. DSDP Site 40 recovered 140 m of upper–middle Eocene radiolarian ooze beneath ~10 m of red clay. DSDP Site 41 with a thinner sediment column (34 m of sediment above basalt) contains 16 m of radiolarian ooze below 18 m of red clay. Piston core EW9709-3PC, taken on the site survey for the potential Leg 199 drill Site PAT-13 (19°46′N, 138°55′W), also cored 5 m of middle Eocene radiolarian ooze beneath 10 m of red clay. On the basis of this apparent sharp zonation in tropical biotic communities, a major oceanographic boundary must have existed between the paleoposition of Site 1216 and Sites 40 and 41.

OPERATIONS

Transit to Site 1216 (PAT-26D)

The 534-nmi transit to proposed Site PAT-26D was accomplished in 50.3 hr at an average speed of 10.6 kt. The vessel encountered a moderate current during 5 November, 2001 that reduced the daily average rate to 9.9 kt. At 1645 hr on 5 November, the vessel slowed to 6 kt, and the seismic equipment was deployed. The seismic survey utilized the 80-in^3 water gun and Teledyne hydrophone streamer. The first leg of the survey was an 11-nmi north-northwest to south-southeast traverse across the prospective location. A short crossing track from east-northeast to west-southwest concluded the survey. The 24-nmi survey required 4.2 hr at an average speed of 5.7 kt. Following the retrieval of the seismic equipment, the vessel came about and returned to site, at which time the thrusters were lowered and the dynamic positioning system was activated. The vessel was on the Global Positioning System coordinates of the new location by 2130 hr on 5 November. The hydrophones were then lowered, and assembly of the bottom-hole assembly began. A beacon was deployed at 2141 hr on 5 November.

Hole 1216A

After the drill string was deployed to a depth of 5100 meters below rig floor (mbrf), a "mudline" core was attempted from 5105.4 mbrf and resulted in a "water core," indicating that the bit was >10 mbsf. The next attempt was made at 5115.4 mbrf with the same result. A third attempt was made with the bit at 5125.4 mbrf and a fourth from 5135.4 mbrf, both of which resulted in water cores. The driller then lowered the bit until the heave compensator appeared to activate, suggesting contact with a firm sea bottom at a bit depth of ~5167 mbrf. The sixth attempt at a mudline core was made with the bit at 5163.0 mbrf, and Hole 1216A finally was spudded with the advanced piston corer (APC) at 1615 hr on 6 November. The seafloor depth, indicated by the recovery of the first core, was 5163.3 mbrf, 50 m deeper than the precision depth recorder (PDR) depth. The usual suspects (misreading the PDR, miscounting the drill pipe, applying the wrong Matthew's table correction, and improper addition) were reviewed, but no culprit could be found. The uncorrected depth obtained during the initial site survey was also consistent with the PDR reading. The only viable reason remaining for this depth discrepancy appeared to reside in the presence of a very strong side echo that mimicked a seafloor return on the bathymetric record.

A total of 10 piston cores were taken at Hole 1216A (Table T1). The cores were oriented starting with 3H. The first four piston cores were full-stroke events. All the remaining piston core attempts, however, did not achieve the fully extended 9.5-m stroke of the piston corer, probably because of the prevalence of chert stringers. Cores 5H–10H (37.7–54.3 mbsf) were obtained using the advance-by-recovery method. With this method, the bit position for the next piston core is advanced only to a depth equal to the recovery of the previous core. No heat flow measurements were attempted because of the high probability of damage to the Adara cutting shoe by chert. APC operations in Hole 1216A resulted in 54.3 m cored with 55.11 m recovered (101.5%).

One extended core barrel (XCB) core (11X; 54.3–62.2 mbsf) was acquired before the hole was terminated. The XCB core advanced 7.9 m and recovered 1.36 m (17.2%). The total recovery at Hole 1216A was 56.5 m, representing 90.8% of the cored interval (Table T1).

Hole 1216B

After the bit cleared the seafloor, the vessel was offset 10 m east of Hole 1216A, and Hole 1216B was spudded with the APC at 0540 hr on 7 November. This was a single-core attempt made with the bit at 5158.0 mbrf (5 m shallower than the bit position of Core 1H). The single core recovered 9.75 m, or 102.6%.

After coring operations concluded at Site 1216, the drilling equipment was secured, and the beacon was successfully recovered. The 24-hr transit to the next site (PAT-19A) began at 1545 hr on 7 November.

LITHOSTRATIGRAPHY

At Site 1216, we sampled a 62-m section composed of pelagic clay and chert (Fig. F3). Fifty meters of pelagic clay of Eocene and younger age overlies 12 m of interbedded pelagic clay and chert. The sedimentary section is divided into two lithologic subunits differentiated by the

T1. Coring summary, p. 34.

F3. Lithologic summary, p. 18.

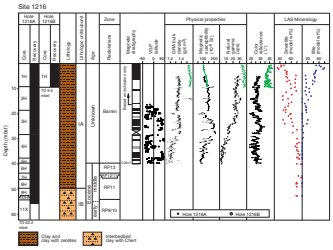

ratio of clay concentration vs. chert. The basal section is intensely affected by drilling disturbance with recovery largely limited to chert fragments. Only one core was recovered at Hole 1216B; therefore, the following lithologic description refers to the more complete sequence from Hole 1216A.

Unit I

Intervals: Cores 199-1216A-1H through 11X and 199-1216B-1H
Depths: 0–62.2 mbsf (Hole 1216A) and 0–9 mbsf (Hole 1216B)
Age: Holocene to Eocene
Lithology: clay, clay with zeolites, and chert

Unit I was divided into two subunits based upon the abundance of chert interbedded with clay.

Subunit IA

Intervals: Cores 199-1216A-1H through 8H and 199-1216B-1H
Depths: 0–49.8 mbsf (Hole 1216A) and 0–9.5 mbsf (Hole 1216B)
Age: Holocene to Eocene
Lithology: clay and clay with zeolites

Subunit IA is composed of pelagic clay. The first two sections of Core 199-1216A-1H contain sediments that alternate between dark brown (10YR 3/3) and brown (10YR 4/3). At the base of Section 199-1216A-1H-2, the color grades to very dark brown (10YR 2/2) and remains this color downcore. Subunit IA is also marked by thin accumulations of altered ash, zeolites, and zeolite clay layers that are yellowish brown (10YR 3/6) in color. Pronounced layers of zeolite accumulations are present in Sections 199-1216A-2H-2 (14 mbsf), 3H-1 (20 mbsf), and 3H-2 (22 mbsf). Zeolites are also abundant in burrow infillings in Core 199-1216A-4H. Both micro- and macromanganese nodules are present in the upper 20 m, and a discontinuous manganese hardground is present at 39 mbsf. Both iron oxide micronodules and black (N1) chert fragments are present in the basal portion of Subunit IA, beginning at 40 and 45 mbsf, respectively.

Subunit IB

Intervals: Cores 199-1216A-9H through 11X
Depths: 49.8–62.2 mbsf (Hole 1216A)
Age: Eocene
Lithology: interbedded pelagic clay/chert

Subunit IB is differentiated from Subunit IA by the predominance of chert. The chert occurs as gravel-sized black (N1) fragments. Chert fragments result from brecciation of layers and/or nodules during drilling. Clay interlayered with the chert is not in situ because of drilling disturbance and in many instances is completely removed.

Discussion/Summary

Site 1216 consists of a 62.2-m interval of pelagic brown clay and black chert, which have accumulated over the past 52 m.y. (see **"Siliceous Microfossils,"** p. 6, in "Biostratigraphy"). Core recovery was excellent in the upper four cores and decreases downcore because of the

increasing frequency of chert. In contrast to Site 1215, there is no pronounced evidence for cyclical sedimentation or marked color changes representing critical transitions in Unit I.

BIOSTRATIGRAPHY

The red clays of Site 1216 (Subunit 1A; Fig. **F3**) are barren of calcareous microfossils. Biostratigraphic control was provided by shipboard analysis of sporadic occurrences of silicious microfossils in the lower part of Hole 1216A (Fig. **F4**). The assemblages encountered indicate an early Eocene–middle Eocene age for these sediments. The fossil content of the upper part of the sequence is limited to ichthyoliths and occasional concentrations of agglutinated benthic foraminifers. The single core recovered from Hole 1216B (Core 199-1216B-1H) contained only ichthyoliths.

F4. Distribution of biostratigraphic zones for radiolarians, p. 19.

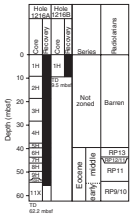

Siliceous Microfossils

Radiolarians were found in Samples 199-1216A-6H-1, 40–42 cm, through 11H-CC (Table **T2**). However, they are never common, preservation is generally poor, and only in Core 199-1216A-6H are they moderately well preserved. It was difficult to disaggregate the clay component of the samples, and in most cases, NaOH was used in addition to the usual cleaning process (Sanfilippo et al., 1985). Zonal designations are somewhat tentative because the absence of certain species may be a reflection of poor preservation rather than true faunal composition.

Sample 199-1216A-6H-1, 40–42 cm, and slurry from Section 6H-3 contain *Eusyringium lagena* and an early form of *Eusyringium fistuligerum,* thus placing the samples in middle Eocene Zone RP13 (Sanfilippo and Nigrini, 1998). The last occurrence of *Thyrsocyrtis hirsuta* appears to be in Sample 199-1216A-7H-1, 47–49 cm, suggesting that this sample belongs to either Zone RP12 or RP11. The next relatively reliable datum is the first occurrence of *Dictyoprora mongolfieri* in Sample 199-1216A-9H-CC, which requires that all samples between Cores 199-1216A-9H and 7H lie within Zone RP11. The presence of *Buryella clinata* in Sample 199-1216A-11X-CC, together with the absence of *Thyrsocyrtis rhizodon,* places that sample in uppermost Zone RP9 or lowermost RP10. These zones straddle the lower/middle Eocene boundary.

T2. Distribution of radiolarians, p. 35.

Benthic Foraminifers

Benthic foraminiferal assemblages at Site 1216 are composed of agglutinated forms only. Calcareous benthic foraminifers were not found in any of the samples examined. The taxa identified are long ranging (Cretaceous–Holocene) and cosmopolitan and, therefore, of little stratigraphic utility. Species diversity of foraminiferal assemblages is low, and species identification is problematic because of poor preservation and fragmentation of the delicate tests during sample preparation. The distribution of benthic foraminifers is reported in Table **T3.**

Samples 199-1216A-1H-CC through 3H-CC and 10H-CC through 11X-CC are barren of benthic foraminifers. Samples 199-1216A-4H-CC and 5H-CC are dominated by agglutinated forms. The assemblages are mainly characterized by *Amodiscus* sp., *Bathysiphon* sp., *Trochamminoides proteus,* and *Glomospira gordialis*. *Miliammina* sp. is also frequently present. These taxa indicate bathyal to abyssal paleodepths. Sample

T3. Distribution of agglutinated benthic foraminifers, p. 36.

199-1216A-6H-3, 104–106 cm, contains poorly preserved and fragmented benthic foraminifers. Assemblages from Samples 199-1216A-7H-CC and 8H-CC are less diverse than those from Samples 4H-CC and 5H-CC, but the dominant taxa are the same as in previous samples, indicating similar paleodepths. Benthic foraminifers are not found in Sample 199-1216B-1H-CC.

PALEOMAGNETISM

The archive-half core sections from Holes 1216A and 1216B were measured on the shipboard pass-through cryogenic magnetometer, except sections that were clearly disturbed by drilling in Cores 199-1216A-6H through 10H and 11X. The natural remanent magnetization (NRM) was measured at 5-cm intervals in each core section, followed by alternating-field (AF) demagnetization at 5, 10, 15, and 20 mT peak field. No discrete samples were demagnetized at this stage. Most of the measured cores displayed consistent remanent inclination and declination directions. NRM intensities were in the order of 10^{-1} to 10^{-2} A/m and decreased to about 10^{-3} to 10^{-2} A/m after partial AF demagnetization at 20 mT (Fig. F5), similar to those of Site 1215. Uncleaned NRM inclinations have steep downward directions of ~80°, indicative of a strong drilling-induced overprint. This overprint was partially removed and typically disappeared after AF demagnetization at 10–15 mT. For the characteristic remanent magnetization (ChRM), we have used the directions obtained after a blanket demagnetization at 20 mT, although the magnetic directions did not reach a stable point suggesting that the ChRM has been only partially isolated. A more reliable ChRM might be obtained by vector analysis of the measured data and shore-based measurements.

F5. Magnetization intensities after AF demagnetization, p. 20.

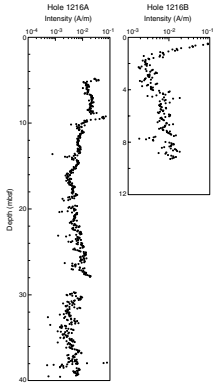

Orientation

The Tensor tool was used to orient cores collected from Hole 1216A starting with Core 199-1216A-3H. The single core from Hole 1216B was not oriented. The orientation was successful in aligning the declinations between most cores as shown in Figure F6. The corrected declinations of the magnetic vectors were very useful in assessing polarity changes, otherwise the inclinations by themselves would produce an ambiguous record as a result of the low paleolatitude of this site.

F6. Comparison of uncorrected and corrected declinations, p. 21.

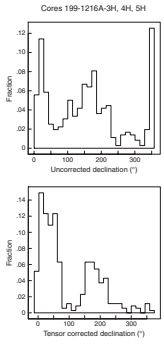

Discrete Sample Analysis

Bulk magnetic susceptibility (MS) was measured on discrete samples taken from Hole 1216A, but no demagnetization was attempted.

Magnetic Polarity Stratigraphy

The magnetic declinations of the oriented cores are relatively well behaved and are grouped in two antipodal clusters (Fig. F6) with a prevalence of northward directions. In the measured archive halves of Hole 1216A, the 20-mT AF demagnetization directions have an average inclination value around 35° with large scatter (σ = 20). Despite the average inclination value, many samples, especially in the upper 15 mbsf of Hole 1216A, have rather steep inclinations that are not compatible with either the present field inclination or the paleolatitude of the site. We speculate that coring in soft sediment might have affected the inclina-

tions by physically reorienting the sediment close to the core edges to a nearly vertical direction. In addition, the magnetic field inside the barrel produces a secondary overprint on the sediments. These hypotheses need to be further explored in postcruise analyses comparing discrete samples taken from the middle and external parts of the core.

No paleomagnetic record was obtained from the top 5 m in Hole 1216A because of core disturbance. Furthermore, the major change in the inclination record in the upper part of Hole 1216A (at 10 mbsf) cannot be unambiguously interpreted.

In oriented cores below 19 mbsf in Hole 1216A, the magnetic polarity has been computed by the virtual geomagnetic pole (VGP) latitude that combines the information from both inclinations and declinations. Because of the quality of the declination record in this site, the VGP latitude is very effective in outlining several geomagnetic reversals (Fig. F7) although the interpretation of the magnetic chrons is not unequivocal. Based on the radiolarian zonation (Zone RP13), we believe that Chron C20n can be found at the base of Core 199-1216A-5H at ~40 mbsf.

F7. Magnetic stratigraphy, p. 22.

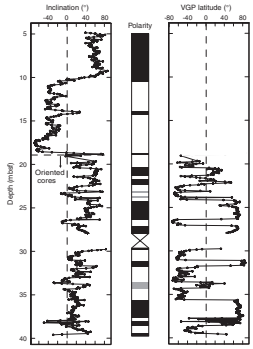

COMPOSITE DEPTHS

Hole 1216A extended to a depth of 55.66 mbsf. Cores 199-1216A-5H through 11X were highly disturbed and recovered mostly chert fragments. Only one core was recovered from Hole 1216B, after which Site 1216 was abandoned. Therefore, it was not possible to generate composite depth or spliced records for Site 1216. Here, we present a comparison of cleaned and culled Site 1216 MST and color reflectance data to spliced records from Site 1215.

MST and color reflectance data were collected from Holes 1216A and 1216B. MS, *P*-wave velocity, and color reflectance data were collected at 2-cm intervals and gamma ray attenuation (GRA) bulk density at 4-cm intervals on all cores recovered from Holes 1216A and 1216B (see "Physical Properties," p. 12, and "Lithostratigraphy," p. 4, for details about MST and color reflectance data). Cores 199-1216A-5H through 11X recovered mostly chert fragments, and MST data from these cores are unreliable. Table T4 lists intervals from Holes 1216A and 1216B that are interpreted to be disturbed and are excluded from further discussion.

T4. Core disturbance table, p. 37.

Figure F8 illustrates the MST and color reflectance data from Site 1216 on an mbsf depth scale after culling intervals given in Table T4. On the basis of MST and color reflectance data alone, it is not possible to reliably determine a depth offset between Hole 1216A and 1216B. The MS data from Hole 1216B have different absolute values, most likely attributable to core disturbance in the upper intervals of both holes. Compressional wave–velocity data from both holes exhibit an apparent 1.5-m cyclicity directly correlatable to the 1.5-m section breaks within the cores. The cyclicity is an artifact of the core-sectioning process that results in a reduction of porosity toward the ends of core sections. Paleomagnetic intensity data suggest, however, that Hole 1216A should probably be offset downward with respect to Hole 1216B by ~3 m (see "Paleomagnetism," p. 7).

F8. GRA bulk density, MS, color reflectance, *P*-wave velocity, and natural gamma total count data plotted vs. depth, p. 23.

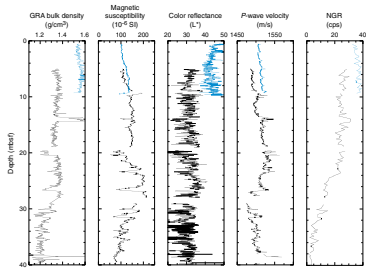

At Site 1216, the MST-NGR data (Fig. F8) have a trend that is very similar to that expressed at Site 1215. Based on the NGR and MS data, an attempt was made to correlate MST data recovered from Site 1216 with those from Site 1215. The correlation of data between Sites 1215

and 1216 was performed using the software package Analyseries (version 1.2) (Paillard et al., 1996). The strategy chosen was to maximize the fit between the MS data from Site 1216A and the spliced records from Site 1215, also taking into consideration paleomagnetic data that suggest a reversal in polarity at ~10 mbsf in Hole 1216A can also be identified at ~2 mbsf in Hole 1215A (2.8 meters composite depth [mcd]). Data points from Hole 1216A were linearly interpolated between these ties. The resulting match can be evaluated in Figure **F9,** which also shows the location of tie points and their corresponding depth. The points at which data from both sites were matched are also given in Figure **F9.** With respect to the mcd scale of Site 1215, the linear sedimentation rate (LSR) of Hole 1216A (on an mbsf scale) is approximately a factor of 1.6 greater to a depth of 22 mbsf and approximately similar to that of Site 1215 from 22 to 37.5 mbsf in Hole 1216A (Fig. **F9**).

SEDIMENTATION AND ACCUMULATION RATES

Average LSRs at Site 1216 are based primarily on paleomagnetic reversals and radiolarian zonal boundaries as defined in Hole 1216A (Tables **T5, T6,** respectively). Because only one core was taken at the top of Hole 1216B, no composite depth for the site was calculated. LSR values are combined with the dry bulk density (DBD) data (from porosity measurements on individual samples, averaged over the intervals reported) (see **"Physical Properties,"** p. 12) (Table **T11**) to determine the mass accumulation rates (MARs) of the sediments.

The paleomagnetic inclination data (see **"Paleomagnetism,"** p. 7) (Fig. **F7**) show one comparatively long normal event at the top of Hole 1216A. The base of this event at 10 mbsf, if it represents the base of Subchron C1r.1n (Jaramillo), would have an age of ~1 Ma. The magnetic reversal data are very compressed because of the low sedimentation rates in the pelagic clay facies; thus, it is difficult to recognize the standard magnetic reversal chronology. However, based on the presence of radiolarians from Zone RP13 in Core 199-1216A-6H (see **"Biostratigraphy,"** p. 6) (Table **T3**), it is thought that the reversal near the base of Core 199-1216A-5H (see **"Paleomagnetism,"** p. 7) (Fig. **F7**) may be the top of Chron C20n, and the base of the long normal section above the overlying reversed interval may be the base of Chron C19n. These very tentative magnetic reversal identifications are used together with three identified radiolarian zonal boundaries (Tables **T5, T6**) to establish the sedimentation rates for Site 1216 (Fig. **F10**).

By combining LSR values with DBD data, we determined the MAR of the total sediment (Table **T7**). Sediment with an LSR of 1.0 cm/k.y. and a DBD of 1.0 g/cm³ will have a MAR value of 1.0 g/cm²/k.y. The observed values are rarely this high, so we report the data in milligrams per square centimeter per thousand years (mg/cm²/k.y.).

Lithologic Subunit IA, pelagic clay, is characterized by two LSR values. DBD values range from 0.3 to 0.55 g/cm³ in this unit. Fluxes are high at the top, averaging ~500 mg/cm²/k.y. for this uppermost 1-m.y. interval, if the uppermost normal paleomagnetic interval does represent Chron C1n through Subchron C1r.1n. These values are significantly higher than MAR values reported elsewhere for this facies (J.D. Gleason, et al., unpubl. data; Kyte et al., 1993; Janecek and Rea, 1983). MAR values for the bulk of the pelagic clay unit range from 20 to 40 mg/cm²/k.y., a more normal range for pelagic "red" clays.

F9. Plot of GRA bulk density, MS, and natural gamma count data from Hole 1216A, matched to the spliced data from Site 1215, p. 24.

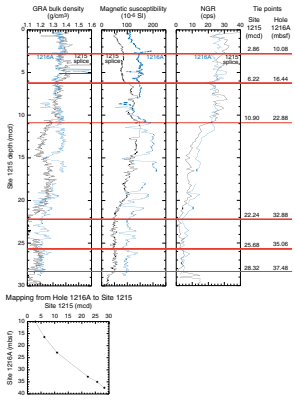

T5. Paleomagnetic events, p. 38.

T6. Radiolarian events, p. 39.

F10. Plot of biostratigraphic and paleomagnetic datum levels vs. mbsf, p. 25.

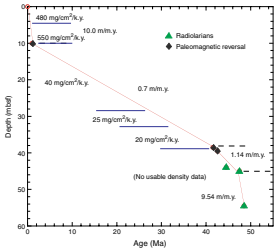

T7. Linear sedimentation rates and mass accumulation rates for the major lithologic units, p. 40.

GEOCHEMISTRY

Interstitial Water Geochemistry

We collected interstitial waters from five samples in Hole 1216A at depths ranging from 4.45 to 47.65 mbsf (Table T8; Fig. F11). However, major ion concentrations of the interstitial water sample taken from 47.65 mbsf indicate contamination with seawater, most likely caused by the incomplete core recovery and the resulting contact with seawater (this sample is not plotted in Fig. F11). Similar to results from Site 1215, chemical gradients in the interstitial waters at this site primarily reflect the limited amount of organic matter diagenesis, the generally nonbiogenic character of the sediments, and possibly a small diffusive signal of chemical reactions in the underlying basalt.

Chlorinity, as measured by titration, increases with depth from values around standard seawater (559 mM) at 4.45 mbsf to values of 564 mM at 32.65 mbsf (Fig. F11). Sodium concentrations determined by charge balance were, on average, 2% lower than those measured by ion chromatograph. Sodium concentrations as determined by charge balance generally remain steady at values similar to that of average seawater. Salinity, as measured by a handheld refractometer, did not vary downcore; all interstitial waters were measured as 35.0.

Alkalinity and pH did not vary significantly downcore in noncontaminated samples at Site 1216. Dissolved silica concentrations increase with depth, from values of around 210 µM at 4.45 mbsf to values of ~610 µM at 32.65 mbsf. Dissolved silica concentrations increase more rapidly with depth than at Site 1215, consistent with the presence of radiolarians in deeper cores (from ~40 mbsf).

Interstitial water sulfate concentrations are high (>27 mM) throughout the section, indicating that the amount of labile organic matter available for oxidation is extremely low. Ammonium is a byproduct of organic matter degradation and is present in extremely low levels (<10 µM), consistent with the high sulfate values.

Dissolved manganese concentrations are low throughout the interstitial water profile at Site 1216. Manganese concentrations slightly increase downcore, from levels of ~1 µM at 4.45 mbsf to levels of ~3 µM at 32.65 mbsf. Strontium concentrations are similar to seawater throughout the pore water profile. The absence of a middepth strontium maximum likely reflects the low carbonate content of the sediments. Lithium pore water values are generally low (between 30 and 40 µM) and show a slight increase downcore.

Calcium concentrations in the pore waters from Site 1216 are similar to that of seawater (~10 mM), with a slight increase at 32.65 mbsf to values of ~11 mM. Magnesium concentrations also increase with depth, reaching levels similar to that of seawater at 32.65 mbsf. Magnesium concentrations in the pore waters from the upper three cores from Site 1216 (4.45–23.15 mbsf) are lower than that of seawater, perhaps indicating magnesium uptake in the precipitation of authigenic minerals. Potassium concentrations decrease downcore, consistent with chemical alteration of basement rocks, suggesting that the hydrothermal signal in the pore water magnesium and calcium profiles is masked by the effects of additional processes. Dissolved barium concentrations are low (<0.45 µM) and show no systematic variation with depth. Levels of dissolved boron decrease with depth, from values of ~650 µM at 4.45 mbsf to values of ~530 µM at 32.65 mbsf.

T8. Interstitial water data, p. 41.

F11. Interstitial water geochemical data, p. 26.

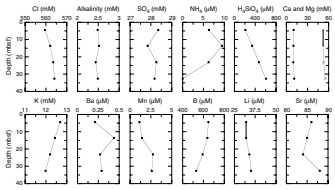

In summary, the pore water profiles from this site primarily reflect the dissolution of biogenic silica, authigenic mineral precipitation, possible alteration of underlying basalt, and subsequent diffusion. High levels of sulfate and concomitant low levels of ammonium suggest a relatively oxic environment, consistent with the occurrences of metalliferous oxides within the sediment. Silica and alkalinity levels in the interstitial waters are higher than seawater values, indicating that biogenic silica was a more important component of the original sedimentary deposits than is obvious by visual inspection of the cores.

Solid-Phase Geochemistry

We collected bulk-sediment samples adjacent to the interval sampled for physical properties (see "Physical Properties," p. 12), resulting in a sampling resolution of approximately one per section from 0.72 to 52.79 mbsf in Hole 1216A (Table T9; Fig. F12). We also collected samples from 1.18 to 8.68 mbsf in Hole 1215B (Table T9). We measured silicon, aluminum, titanium, iron, manganese, calcium, magnesium, phosphorus, strontium, and barium concentrations in the sediment by inductively coupled plasma–atomic emission spectroscopy (ICP-AES). Bulk-sediment geochemistry primarily reflects the predominant red-clay lithology of the sediments.

T9. Bulk-sediment data, p. 42.

F12. Bulk-sediment geochemical data, p. 27.

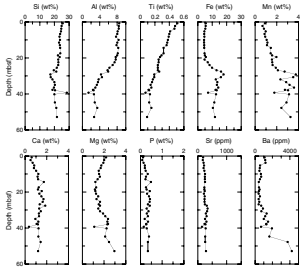

Silicon varies between ~17 and ~25 wt% (Fig. F12). Silicon decreases from ~25 wt% at 0.72 mbsf to ~17 wt% at 29.22 mbsf and is ~22 wt% at 52.79 mbsf. The exception to this trend is a spike of silicon of ~29 wt% at 39.29 mbsf that corresponds to a relative minimum in all other elements measured, presumably because of dilution by the large amount of silicon. Possibly, the sample at 39.29 mbsf may have included a small fragment or nodule of chert.

Aluminum and titanium in Hole 1216A follow similar trends to one another. Between 0.72 and 39.29 mbsf, aluminum decreases from 8.5 to 1.4 wt% and titanium decreases from 0.51 to 0.07 wt%. After reaching minimum values at 39.29 mbsf, aluminum remains steady at ~2.8 wt%, and titanium remains steady at ~0.12 wt%. The Al/Ti ratio is ~25 and is high relative to the Post-Archean Average Shale value of 16.7 (Taylor and McLennan, 1985) (see Fig. F19, p. 70, in the "Leg 199 Summary" chapter).

Iron contents are relatively constant (~5 wt%) to ~21 mbsf, then increase to a peak of 17.89 wt% at 29.22 mbsf. Below this depth, iron remains at ~12 wt% in the rest of the hole, except for a low of 7.14 wt% at 39.29 mbsf. Manganese increases from 0.91 wt% at 0.72 mbsf to a peak of 3.76 wt% at 29.22 mbsf and for the rest of the hole varies between 1.78 and 3.6 wt%.

Calcium is <2 wt% in the entire hole, consistent with the lack of carbonate. Likewise, strontium is low, at ~200 ppm, throughout. Magnesium decreases from 2.2 wt% at 0.72 mbsf to 1.5 wt% at ~10 mbsf. Subsequently, Mg shows a modest increase downcore to values of almost 3 wt% at 52.79 mbsf, with the exception of a low at 39.29 mbsf.

Phosphorus is uniformly low at <0.5 wt% in Hole 1216A. Barium increases downcore from ~1090 ppm at 0.72 mbsf to a peak value of 4200 ppm at 52.79 mbsf.

Calcium carbonate ($CaCO_3$; in weight percent) and organic carbon (C_{org}) (in weight percent) were determined for approximately two samples per core from Hole 1216 (Table T10). $CaCO_3$ measured by coulometer is low (less than or equal to ~1 wt%) for all of the sediments from

T10. Calcium carbonate and organic carbon data, p. 43.

Site 1216. $CaCO_3$ values calculated from Ca contents (in weight percent) yielded similar trends to $CaCO_3$ measured via coulometer, although absolute values are negative, indicating a problem with the calibration at very low carbonate values (Table **T10**) (see **"Geochemistry,"** p. 20, in the "Explanatory Notes" chapter). C_{org} is uniformly low (0–0.09 wt%) for all samples measured (Table **T10**).

In summary, the bulk geochemistry of the sediments from Site 1216 is very similar to that in the red-clay unit of Site 1215.

PHYSICAL PROPERTIES

Physical properties at Site 1216 were measured on whole cores, split cores, and discrete samples. MST measurements (bulk density, MS, *P*-wave velocity, and natural gamma radiation) and thermal conductivity comprised the whole-core measurements. Compressional wave velocity measurements on split cores and moisture and density (MAD) analyses on discrete core samples were made at a frequency of one per section. Because the first three sections of Core 199-1216A-1H were significantly disturbed, the corresponding interval in Hole 1216B was sampled. LAS analyses were performed on the MAD samples as well as an additional one sample per section (located ~50 cm from the MAD sample).

Density and Porosity

Two methods were used to evaluate the wet bulk density at Site 1216. GRA provided an estimate from whole cores. MAD samples gave a second, independent measure of wet bulk density, along with providing DBD, grain density, water content, and porosity from discrete samples (Table **T11**). MAD wet bulk densities trend ~0.05 g/cm³ higher than the GRA estimated densities in the uppermost 30 m at Site 1216 (Fig. **F13**). Below 30 mbsf the two bulk density measures coincide more closely. Crossplots of wet bulk densities and DBD vs. interpolated GRA density (Fig. **F14**) show that despite the offset in the upper section of the site, the overall match between the data sets is very good.

Wet bulk density values are nearly constant about a mean of 1.41 g/cm³ from the seafloor to 30 mbsf. Between 30 and 35 mbsf, wet bulk density decreases uniformly to 1.19 g/cm³. This shift in density corresponds to the transition from illite-rich to smectite-rich clays as indicated by the LAS analyses. Below 35 mbsf, wet bulk density is more variable and ranges from 1.21 to 1.32 g/cm³. Grain densities are ~2.6 g/cm³ in the uppermost 20 m at Site 1216. Within the interval of 20–29 mbsf, grain density increases downcore to a maximum of ~2.9 g/cm³. This increase may be the result of higher concentrations of Fe and Mn in sediments (see **"Geochemistry,"** p. 10). Below 30 mbsf, there is a large decrease in grain density that is consistent with a change from illite to smectite dominance in the sediment (as indicated by LAS analyses). Omitting an anomalous value of 2.57 g/cm³ at 39.30 mbsf, grain density averages 2.16 g/cm³ in this interval (smectite has a grain density of ~2.2 g/cm³). Porosity is ~75% from the seafloor to 25 mbsf. From 25 to 32 mbsf, it increases to 83%. Below 32 mbsf, porosity remains high, averaging 82%.

T11. Moisture and density, p. 44.

F13. Moisture and density measurements, p. 28.

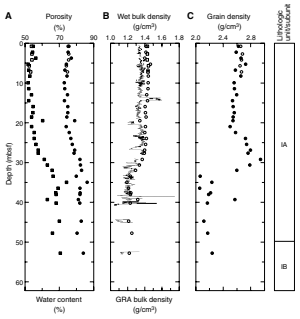

F14. Wet and dry bulk density vs. GRA density, p. 29.

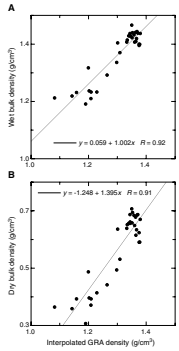

LAS

LAS studies were conducted on cores from Hole 1216A at a frequency of two samples per section (see **Vanden Berg and Jarrard,** this volume, for a discussion of the LAS technique). Semiquantitative mineral concentrations were calculated from the collected spectra, assuming a four-component system: calcite, opal/silica, smectite, and illite (Table **T12**). LAS-derived mineralogical data (Fig. **F15**) show that illite decreases downhole while smectite increases. The illite–smectite transition near 25 mbsf may be the same transition that occurs at 10 mbsf in Hole 1215A. Estimated opal/silica concentrations probably reflect other minerals, such as zeolites, because very little biogenic opal was present at this site (see **"Biostratigraphy,"** p. 6). Calcite is probably overestimated because the clays are barren of calcareous microfossils (see **"Biostratigraphy,"** p. 6) and Ca contents measured by ICP-AES analyses are relatively low (see **"Geochemistry,"** p. 10).

Compressional Wave Velocity

Compressional wave velocity was measured by the *P*-wave logger (PWL) on whole cores from Holes 1216A and 1216B and by the insertion and contact probe systems on split cores from Hole 1216A and Hole 1216B (Table **T13**). Measurements with the insertion probe system were restricted to soft sediments in the uppermost 38 m at Site 1216. The match between the whole-core and split-core measurements is relatively good (Fig. **F16**). The discrete values either coincide with the PWL velocities or are up to 15 m/s higher than whole-core measurements. The general trends in the velocities are an increase from 1485 m/s near the seafloor to 1520 m/s at 23 mbsf, a decrease to ~1505 m/s at 32 mbsf, and higher, more variable velocities below 32 mbsf.

Velocity anisotropy was calculated from longitudinal (z-direction) and transverse (y-direction) measurements provided by the insertion probe system to evaluate burial-induced changes in sediment fabric. The anisotropy ranges from –0.7% to 1.8% (Table **T13**) and averages 0.9%, with no consistent trend with depth.

Thermal Conductivity

Thermal conductivity was measured on the third section of cores from Site 1216 (Table **T14**). The thermal conductivity averages 0.77 W/(m·K). As is the case at Site 1215, there is a general inverse relation relationship between thermal conductivity and porosity at Site 1216.

NGR

NGR was measured on all whole-cores at Site 1216 and displays trends similar to the other physical properties (Fig. **F17**). Between the seafloor and 24 mbsf, NGR values are high, 20 to 32 counts per second (cps), coinciding with the illite-rich pelagic clay. The NGR values decrease to ~2 cps at 35 mbsf and remain at this level to the bottom of Hole 1216A. This change is consistent with the transition to more smectite-rich clay.

T12. LAS-based mineralogy, p. 45.

F15. LAS mineralogy determinations, p. 30.

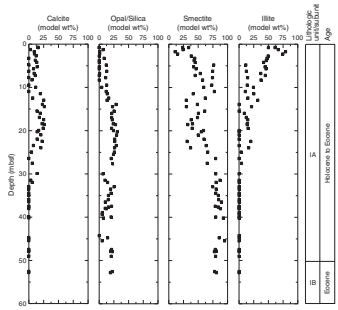

T13. Split-core velocity measurements, p. 46.

F16. Compressional wave velocity and transverse velocity, p. 31.

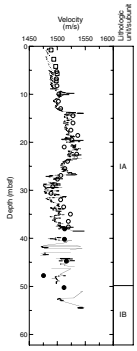

T14. Thermal conductivity, p. 47.

F17. Natural gamma radiation, p. 32.

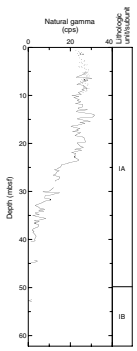

MS

Whole-core MS measurements display greater variability than other properties and do not follow the identified changes in lithology (Fig. F18). The susceptibility increases from 75 × 10^{-6} SI at the seafloor to approximately 200 × 10^{-6} SI at 10 mbsf. Between 10 and 20 mbsf, MS values are more uniform in a range of 125 to 165 × 10^{-6} SI. Below 20 mbsf, the susceptibility is more variable and increases to 215 × 10^{-6} SI at 28 mbsf. A variable, but consistent decrease to 75 × 10^{-6} SI coincides with the proposed transition to more smectite-rich clay between 30 and 40 mbsf. Below this depth, measurements are few as a result of coring disturbance and the MS values are ~75 × 10^{-6} SI.

F18. Magnetic susceptibility, p. 33.

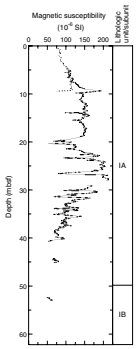

REFERENCES

Atwater, T., and Severinghaus, J., 1989. Tectonic maps of the northeast Pacific. *In* Winterer, E.L., Hussong, D.M., and Decker, R.W. (Eds.), *The Eastern Pacific Ocean and Hawaii*. Geol. Soc. Am., Geol. of North America Ser., N:15–20.

Engebretson, D.C., Cox, A., and Gordon, R.G., 1985. *Relative Motions Between Oceanic and Continental Plates in the Pacific Basin*. Spec. Pap.—Geol. Soc. Am., 206.

Gripp, A.E., and Gordon, R.G., 1990. Current plate velocities relative to the hotspots incorporating the NUVEL-1 global plate motion model. *Geophys. Res. Lett.,* 17:1109–1112.

Janecek, T.R., and Rea, D.K., 1983. Eolian deposition in the northeast Pacific Ocean: Cenozoic history of atmospheric circulation. *Geol. Soc. Am. Bull.,* 94:730–738.

Kyte, F.T., Leinen, M., Heath, G.R., and Zhou, L., 1993. Cenozoic sedimentation history of the central North Pacific: inferences from the elemental geochemistry of Core LL44-GPC3. *Geochim. Cosmochim. Acta,* 57:1719–1740.

Moore, T.C., Jr., Rea, D.K., Lyle, M., and Liberty, L.M., 2002. Equatorial Ocean circulation in an extreme warm climate: *Paleoceanography.* 10.1029/2000PA000566,13.

Paillard, D., Labeyrie, L., and. Yiou, P., 1996. Macintosh program performs time-series analysis. *Eos,* 77:379.

Petronotis, K.E., Gordon, R.G., and Acton, G.D., 1994. A 57 Ma Pacific plate paleomagnetic pole determined from a skewness analysis of crossings of marine magnetic anomaly 25r. *Geophys. J. Int.,* 118:529–554.

Sanfilippo, A., Westberg-Smith, M.J., and Riedel, W.R., 1985. Cenozoic radiolaria. *In* Bolli, H.M., Saunders, J.B., and Perch-Nielsen, K. (Eds.), *Plankton Stratigraphy:* Cambridge (Cambridge Univ. Press), 631–712.

Sanfilippo, A., and Nigrini, C., 1998. Code numbers for Cenozoic low latitude radiolarian biostratigraphic zones and GPTS conversion tables. *Mar. Micropaleontol.,* 33:109–156.

Taylor, S.R., and McLennan, S.M., 1985. *The Continental Crust: Its Composition and Evolution:* Oxford (Blackwell Scientific).

Figure F1. Location of Site 1216 along the Leg 199 transect. In the lower panel, gray shading = water depths >5000 mbsl, red shading = approximate position of magnetic Anomaly C25, the nominal target crust for the 56-Ma transect. Open circles = location of DSDP drill sites.

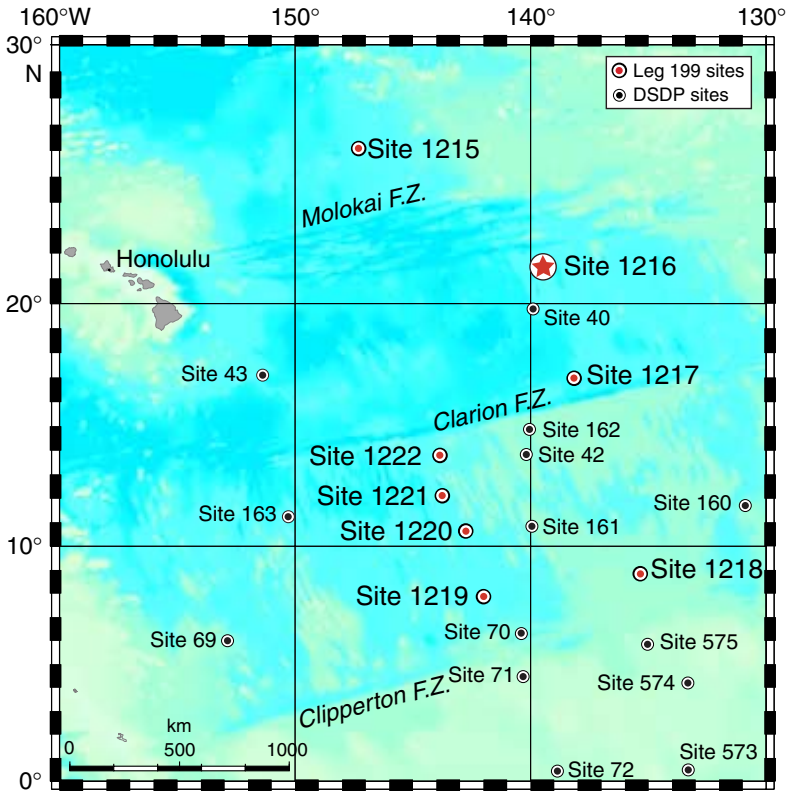

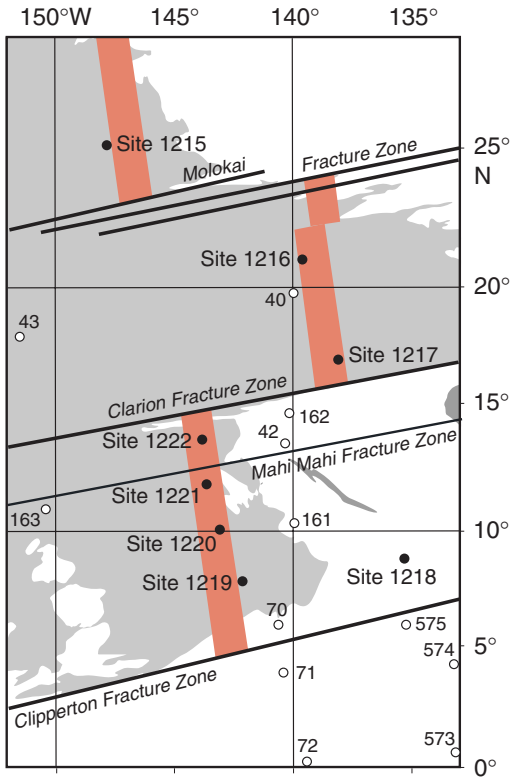

Figure F2. Seismic reflection profile across Site 1216 collected on the EW9709 site survey cruise. The region has thin but continuous sediment cover on abyssal hill topography.

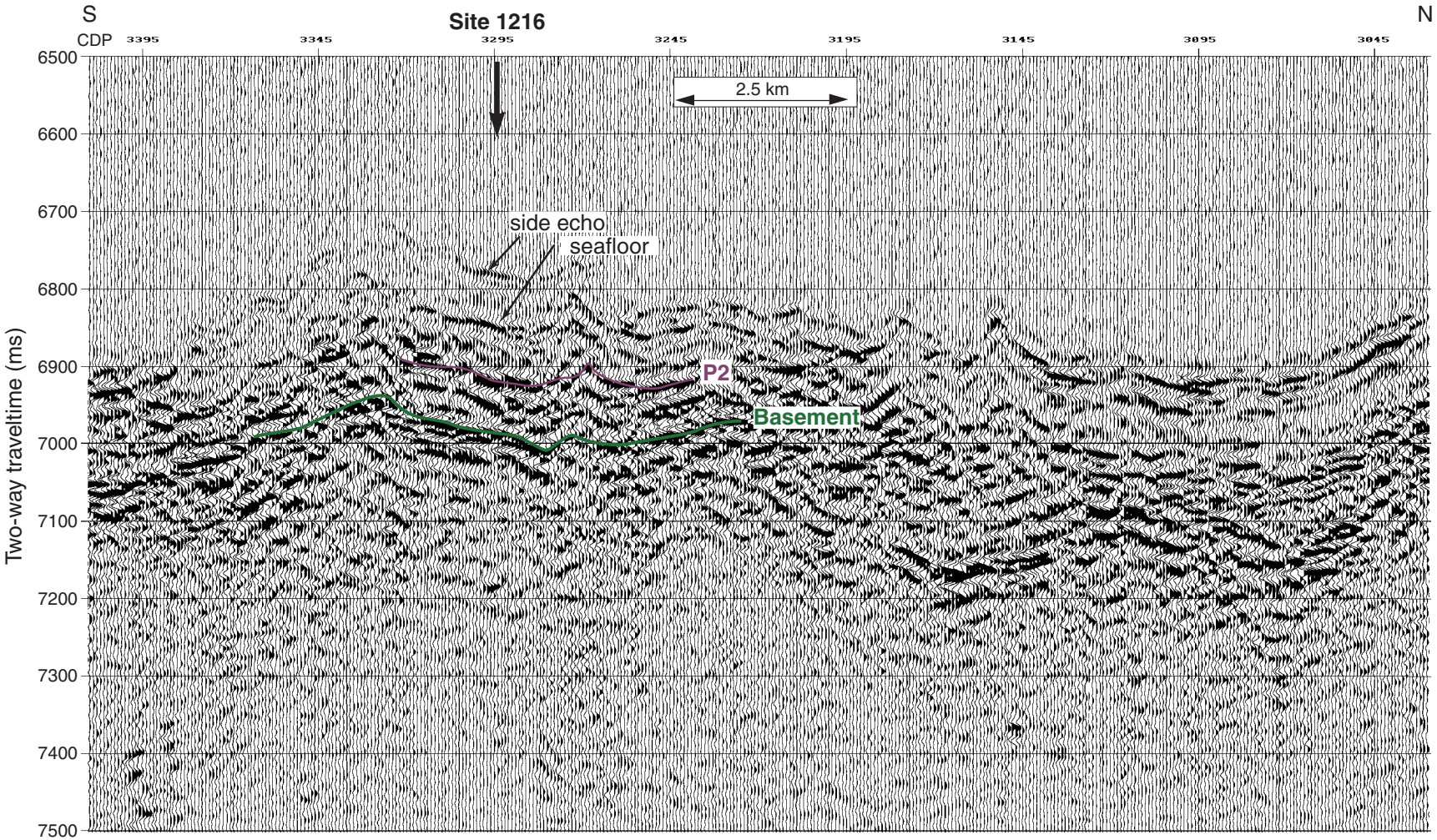

Figure F3. Lithologic summary for Site 1216. VGP = virtual geomagnetic pole, GRA = gamma ray attenuation, LAS = light absorption spectroscopy, cps = counts per second, TD = total depth.

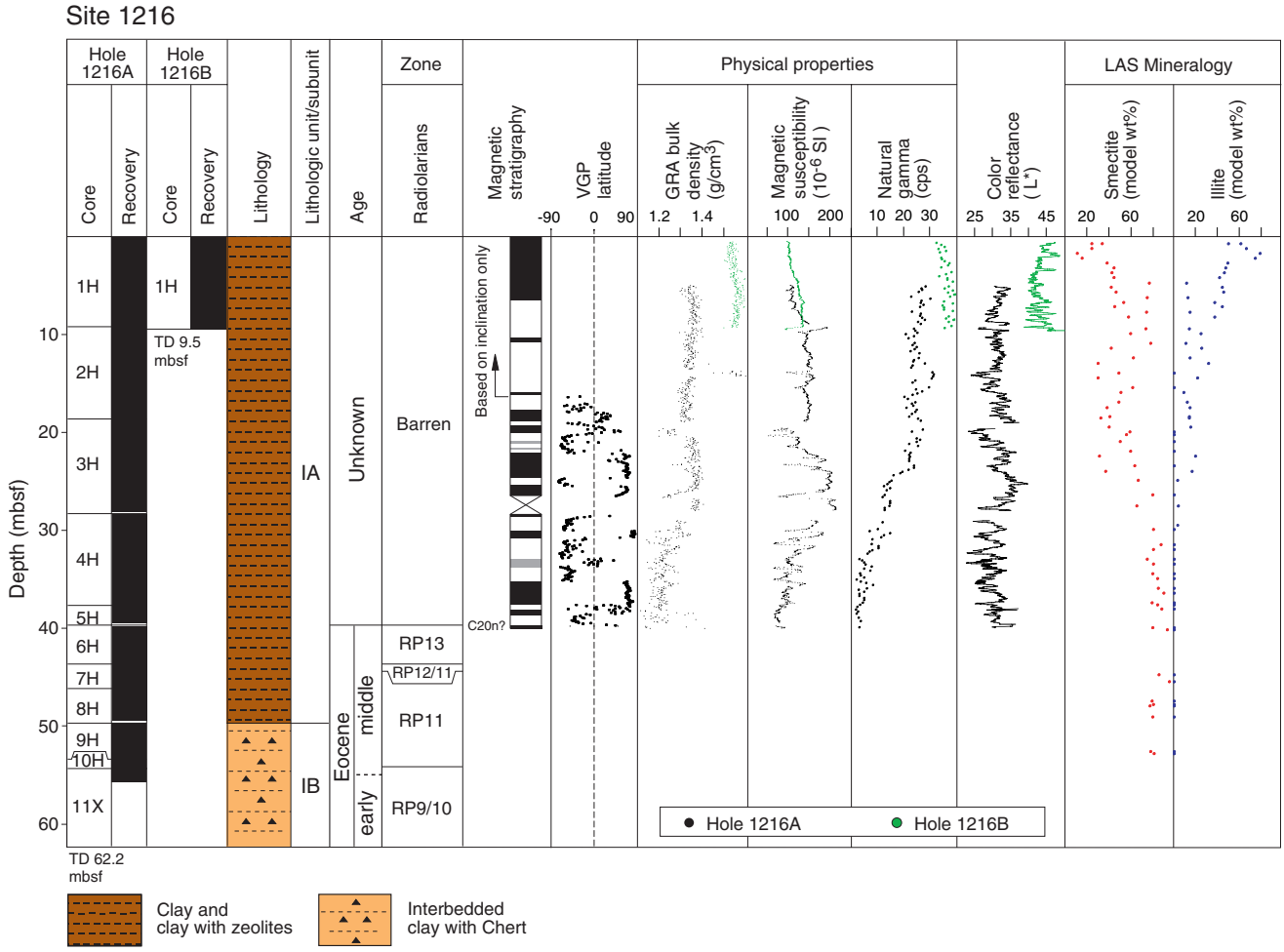

Figure F4. Distribution of biostratigraphic zones for radiolarians at Site 1216. TD = total depth.

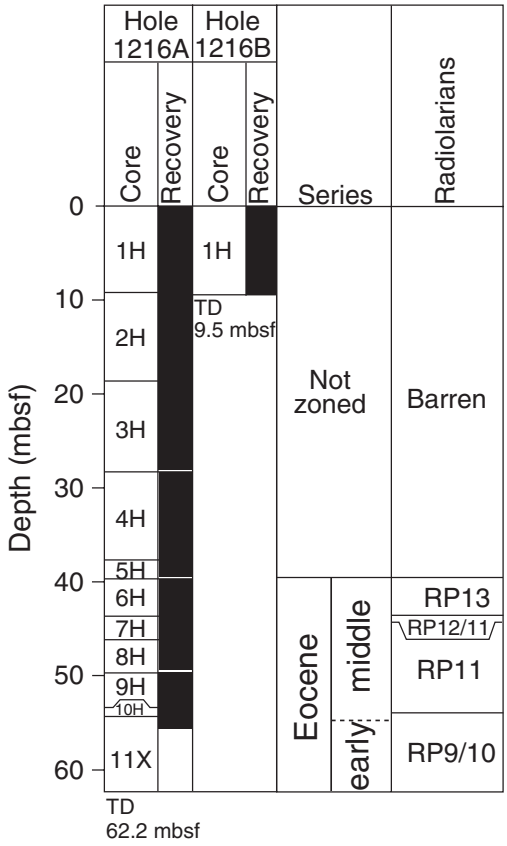

Figure F5. Archive-half magnetization intensities after AF demagnetization at a peak field of 20 mT from Holes 1216A and 1216B.

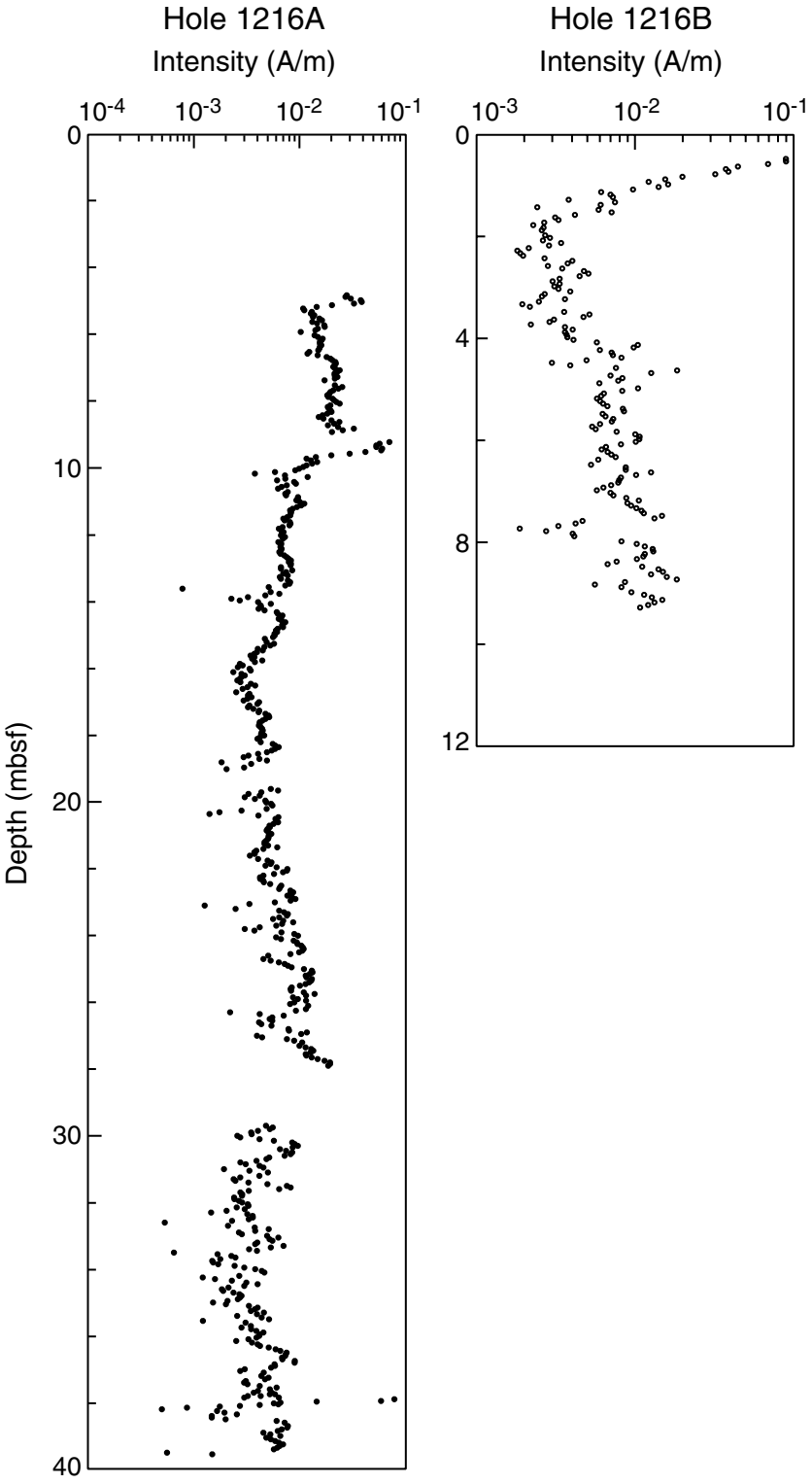

Figure F6. Comparison of uncorrected declinations to declinations corrected using the Tensor orientation tool after partial AF demagnetization at 20 mT. The clustering of the two groups around two approximately antipodal directions reveals the effectiveness of the azimuthal correction.

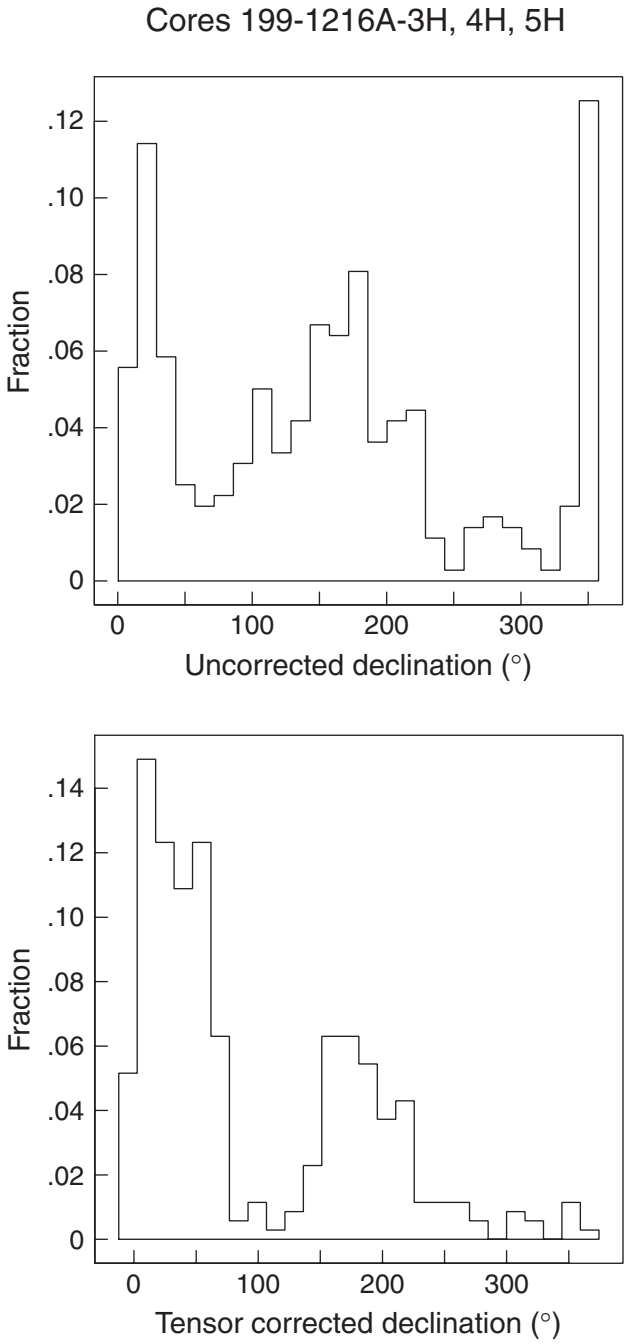

Figure F7. Magnetic stratigraphy at Hole 1216A. Magnetic inclinations and virtual geomagnetic pole (VGP) latitudes were obtained after partial AF demagnetization of continuous measurements at a peak field of 20 mT. Polarity column shows interpreted zones of normal (black) and reversed (white) magnetization; gray intervals indicate zones with an uncertain polarity interpretation.

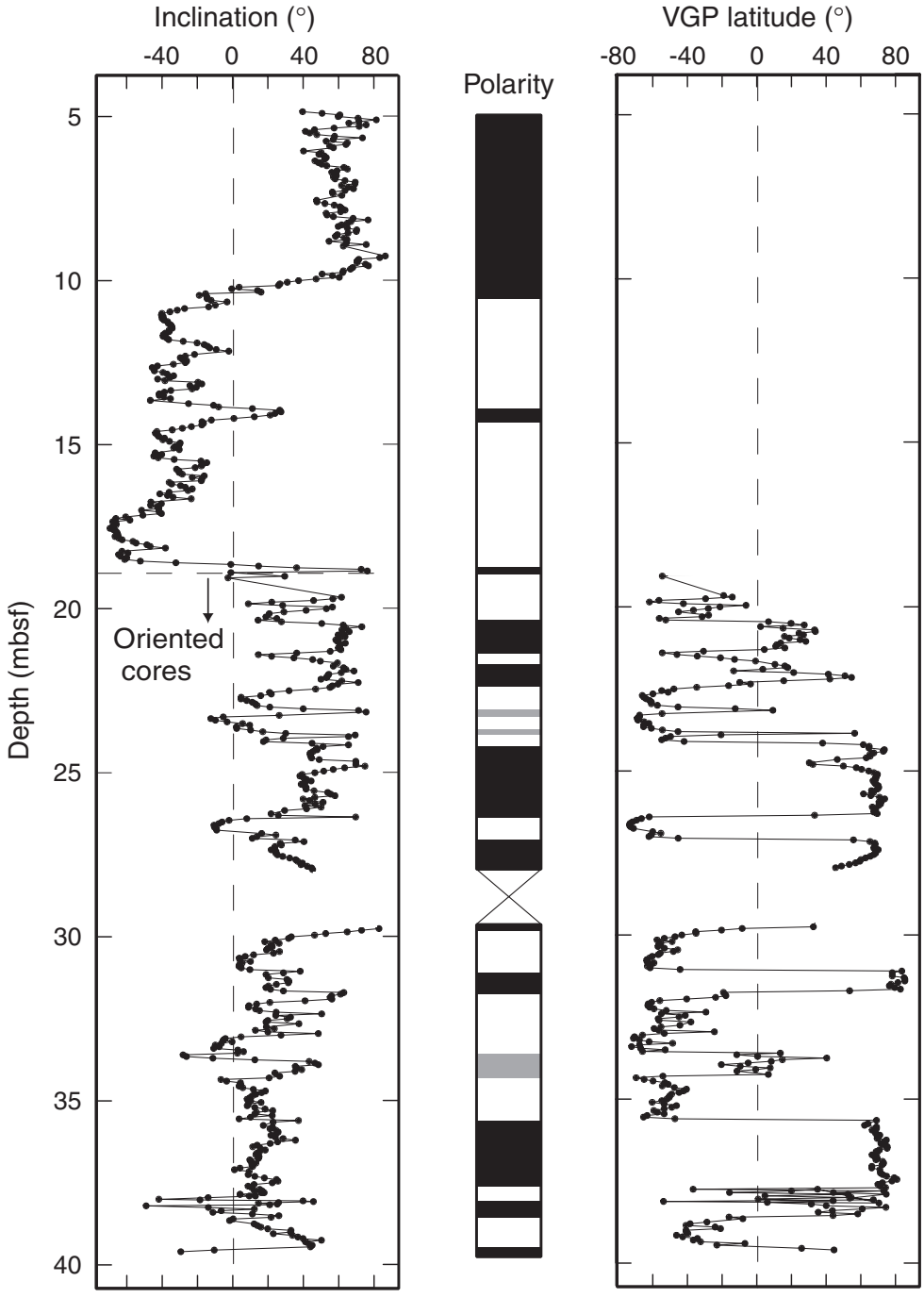

Figure F8. MST data plotted vs. depth for Holes 1216A and 1216B. Gamma ray attenuation (GRA) bulk density, MS, color reflectance, *P*-wave velocity, and natural gamma total count data are shown for Holes 1216A (left curve in each panel) and 1216B (right curve in each panel). The data from Hole 1216B are offset by a constant for illustration purposes. Intervals with obvious flow-in or drilling disturbance were removed from the data sets (see Table **T4,** p. 37). cps = counts per second.

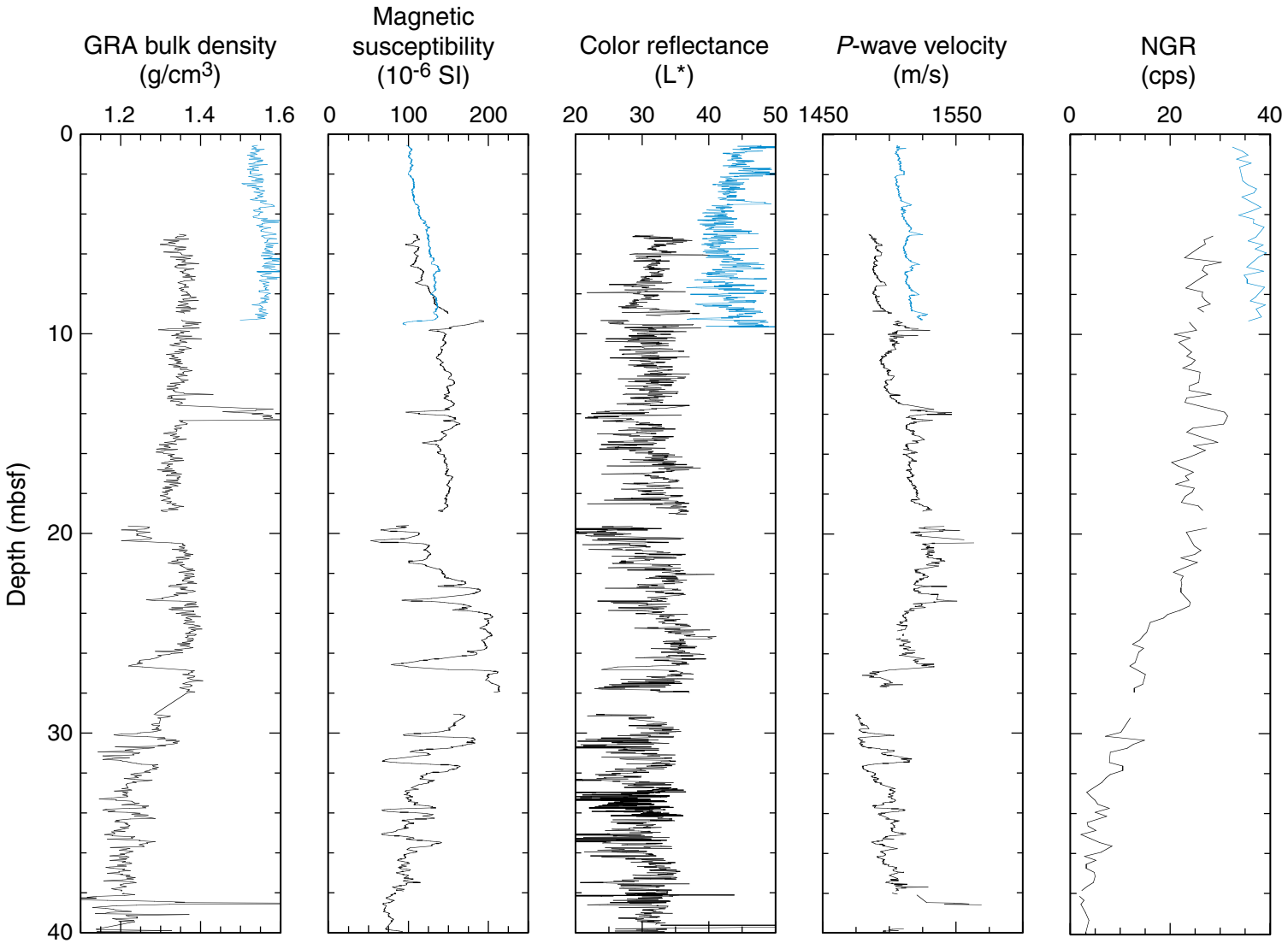

Figure F9. Plot of gamma ray attenuation (GRA) bulk density, MS, and natural gamma count (NGR) data from Hole 1216A, matched to the spliced data from Site 1215. Horizontal lines = tie points (annotated with their corresponding depth intervals). Note that on this correlation, relative stretching and squeezing of the records from both sites was allowed. The bottom panel shows the variation in apparent sedimentation rate changes between the two sites, expressed by the slope of the mapping plot from Hole 1216A mbsf to Site 1215 mcd. cps = counts per second.

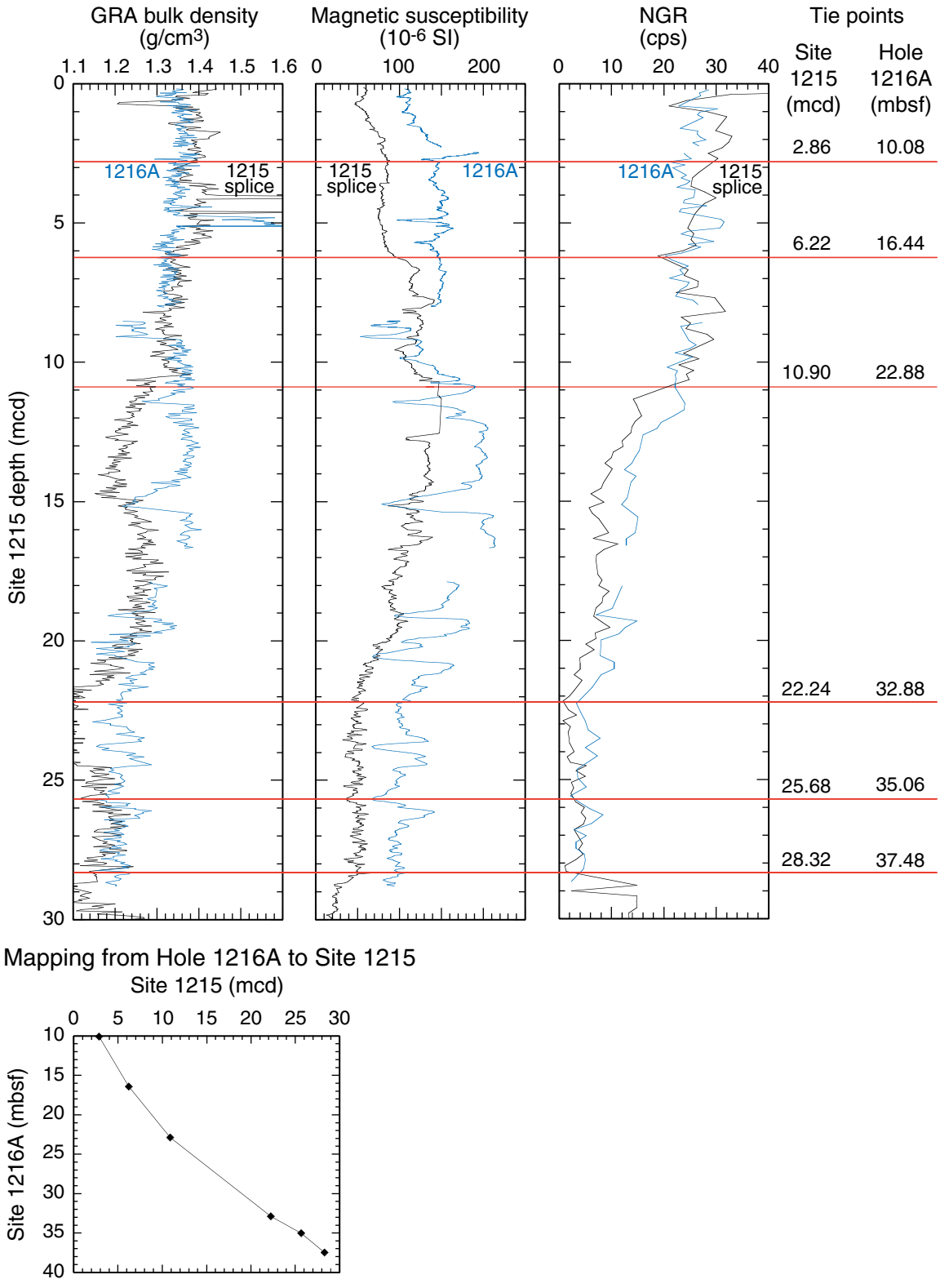

Figure F10. Plot of biostratigraphic and paleomagnetic datum levels (see Tables T5, p. 38, and T6, p. 39) vs. mbsf. Individual symbols represent different types of stratigraphic datums: solid triangle = radiolarians, solid diamond = paleomagnetic reversal. Solid line segments = linear regressions of selected data points with the slope of these lines indicating sedimentation rates in m/m.y. as shown next to each segment. MARs are shown as values in mg/cm²/k.y.

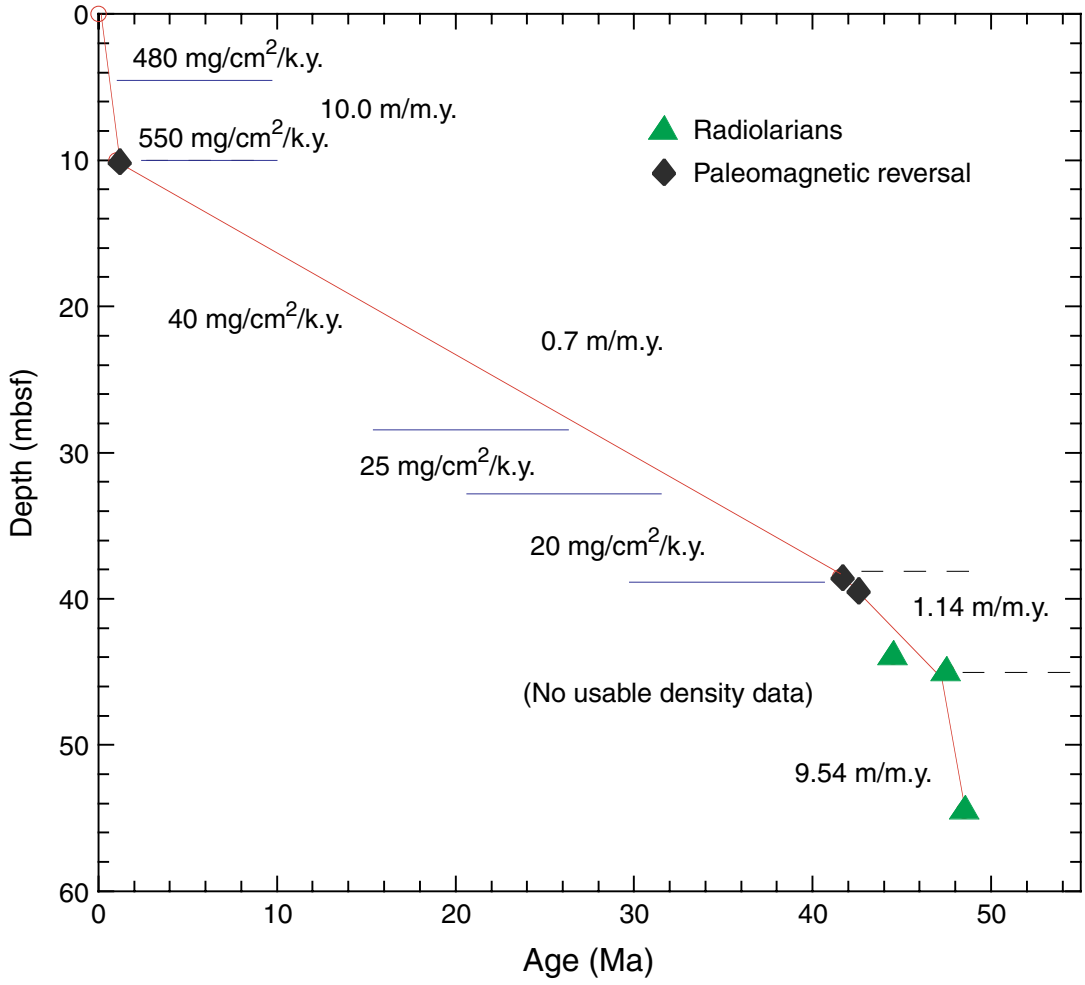

Figure F11. Interstitial water geochemical data from Site 1216. Solid circles = Ca, crosses = Mg.

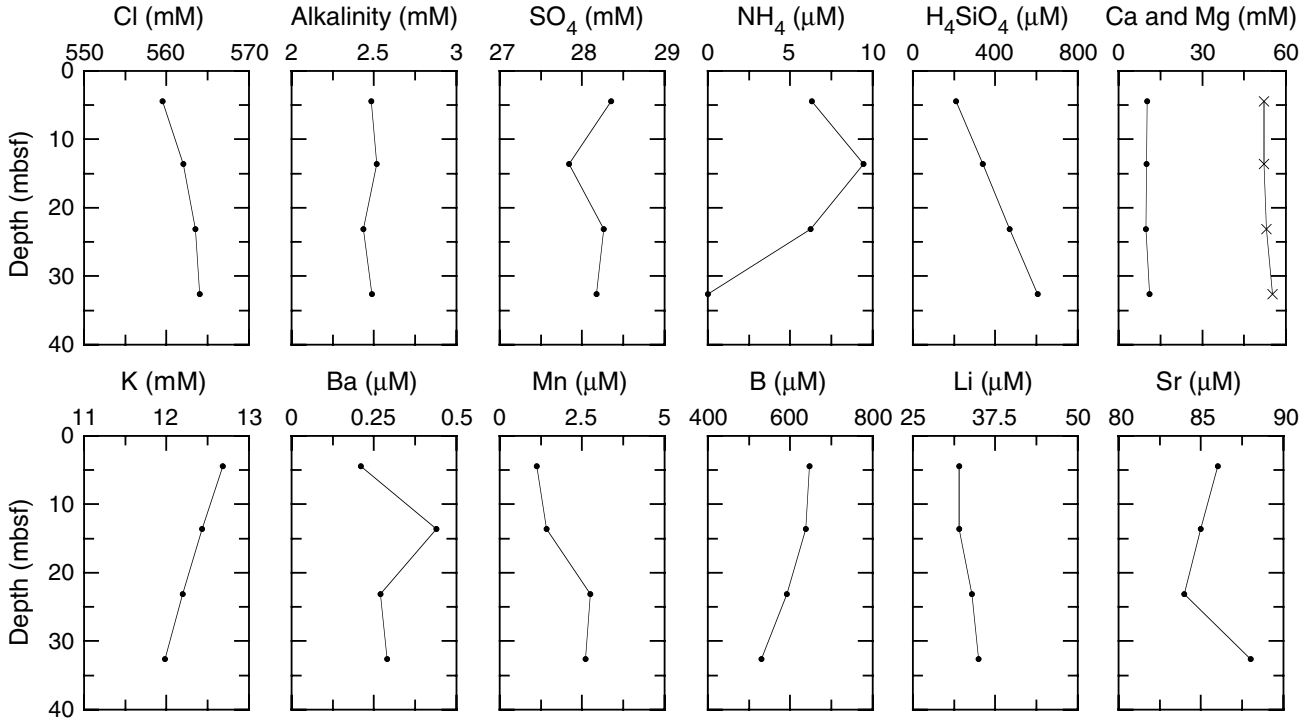

Figure F12. Bulk-sediment geochemical data from Site 1216.

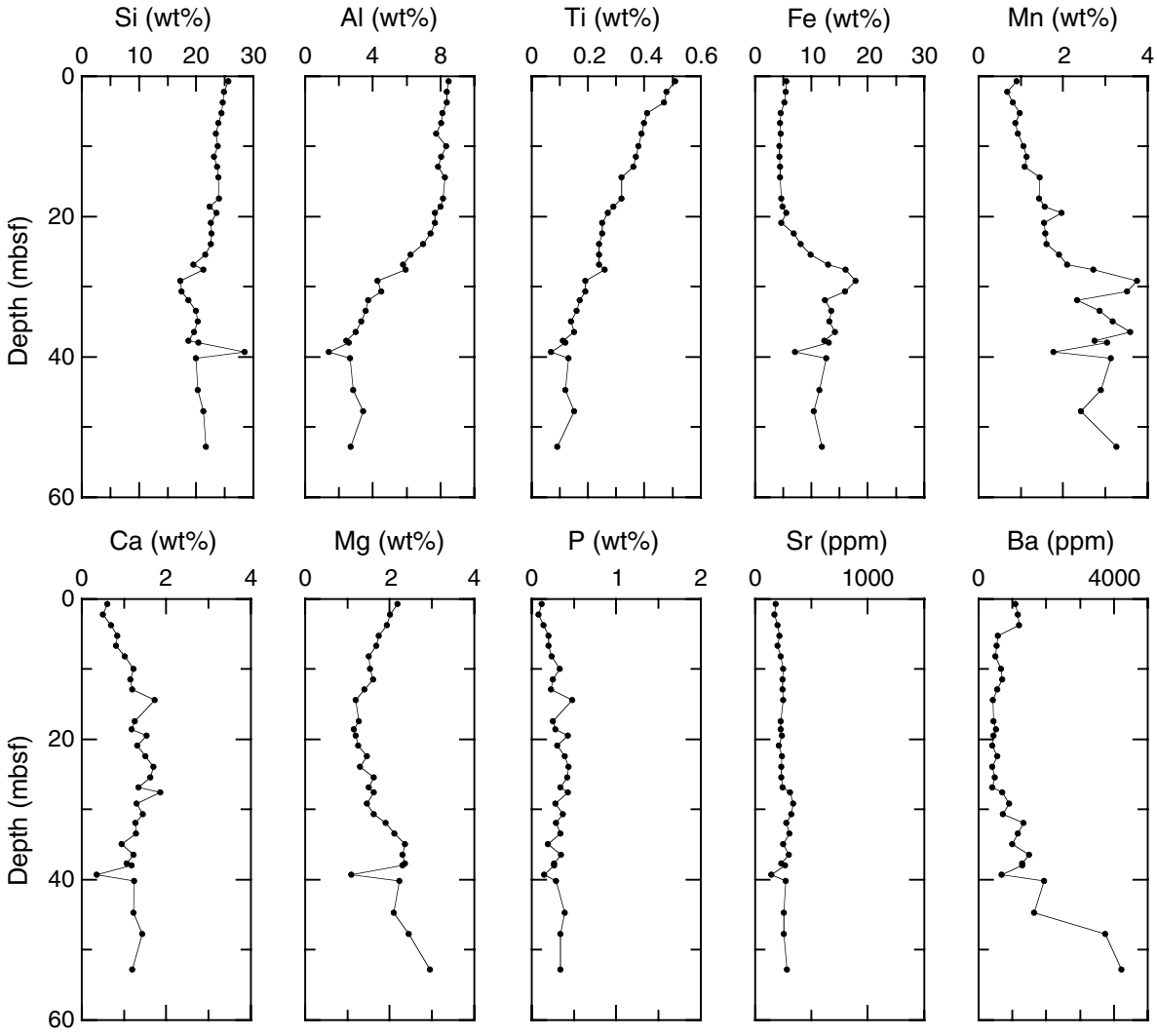

Figure F13. Moisture and density measurements at Site 1216. **A.** Porosity (squares) and water content (circles) for Holes 1216A (closed symbols) and 1216B (open symbols). **B.** Discrete-sample wet bulk density Holes 1216A (open circles) and 1216B (open squares) and gamma ray attenuation (GRA) bulk density, Holes 1216A (solid line) and 1216B (dashed line). **C.** Grain density for Holes 1216A (closed symbols) and 1216B (open symbols). Lithologic Subunits IA and IB are noted on the right side of the figure.

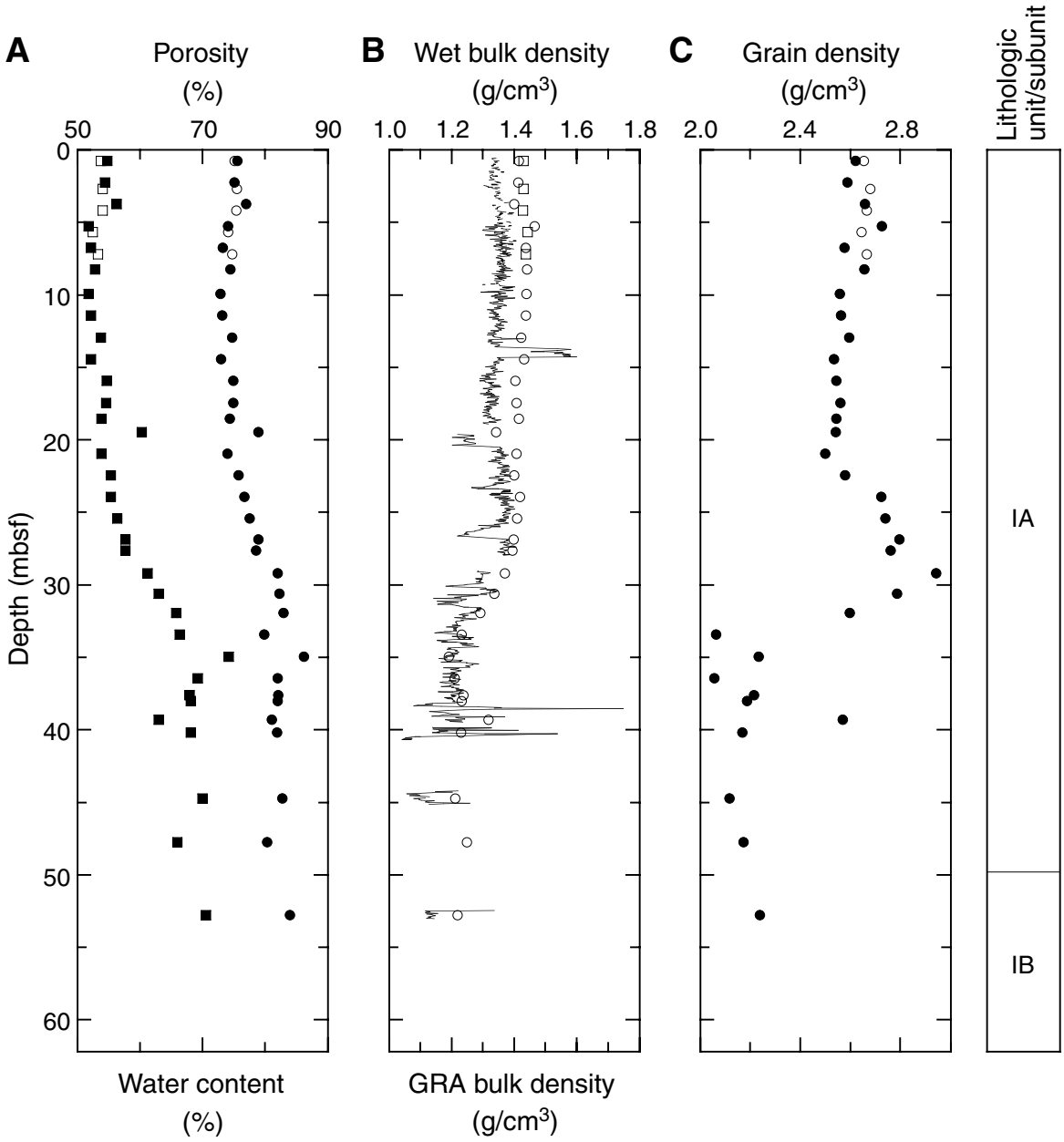

Figure F14. (A) Wet and (B) dry bulk density from discrete samples plotted with gamma ray attenuation (GRA) bulk density interpolated with a 20-cm-wide Gaussian window.

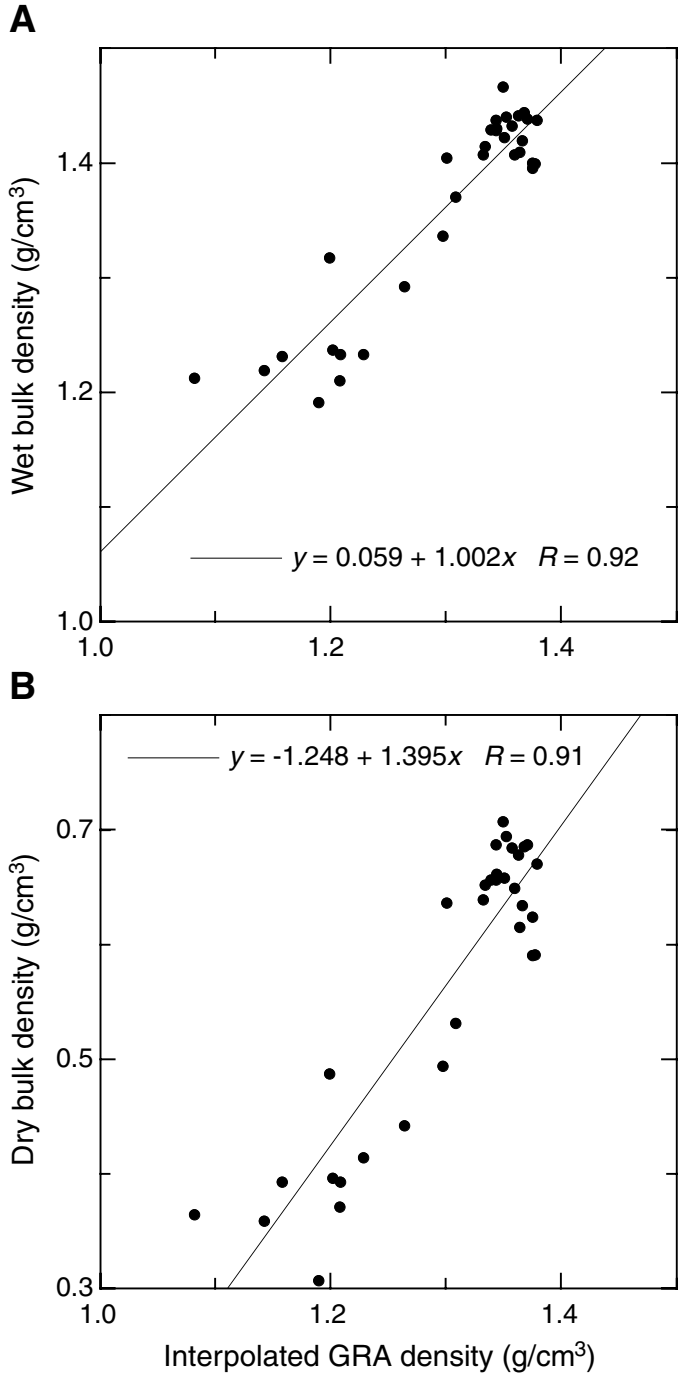

Figure F15. LAS mineralogy determinations for Hole 1216A. Lithologic Subunits IA and IB and relative ages are noted to the right of the figure.

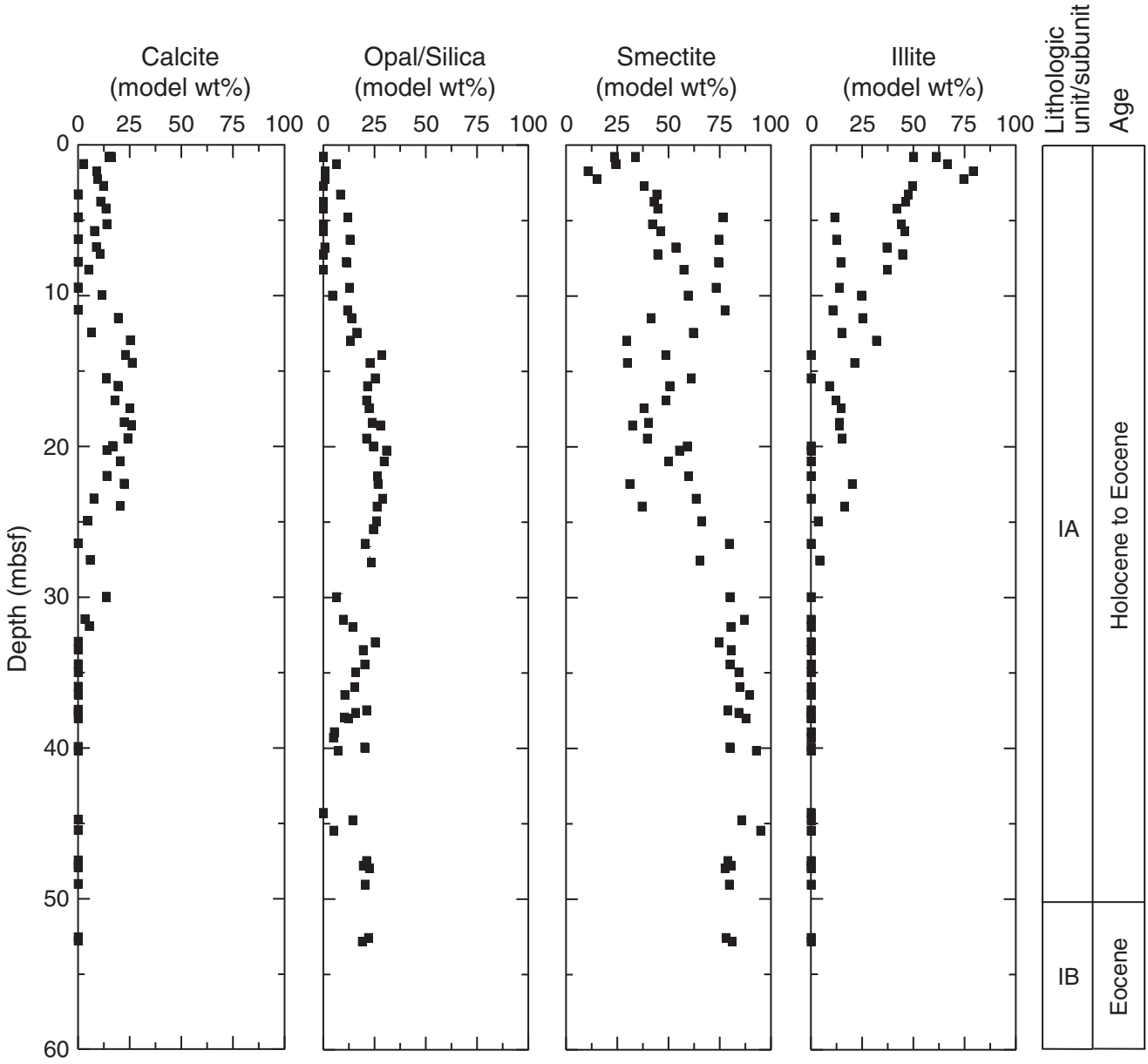

Figure F16. Compressional wave velocity from the PWL (solid line = Hole 1216A, dashed line = 1216B) and transverse velocity measurements of the insertion (open symbols) and contact probe (solid symbols) systems for Site 1216 (circle = Hole 1216A, square = Hole 1216B). Lithologic Subunits IA and IB are noted on the right side of the figure.

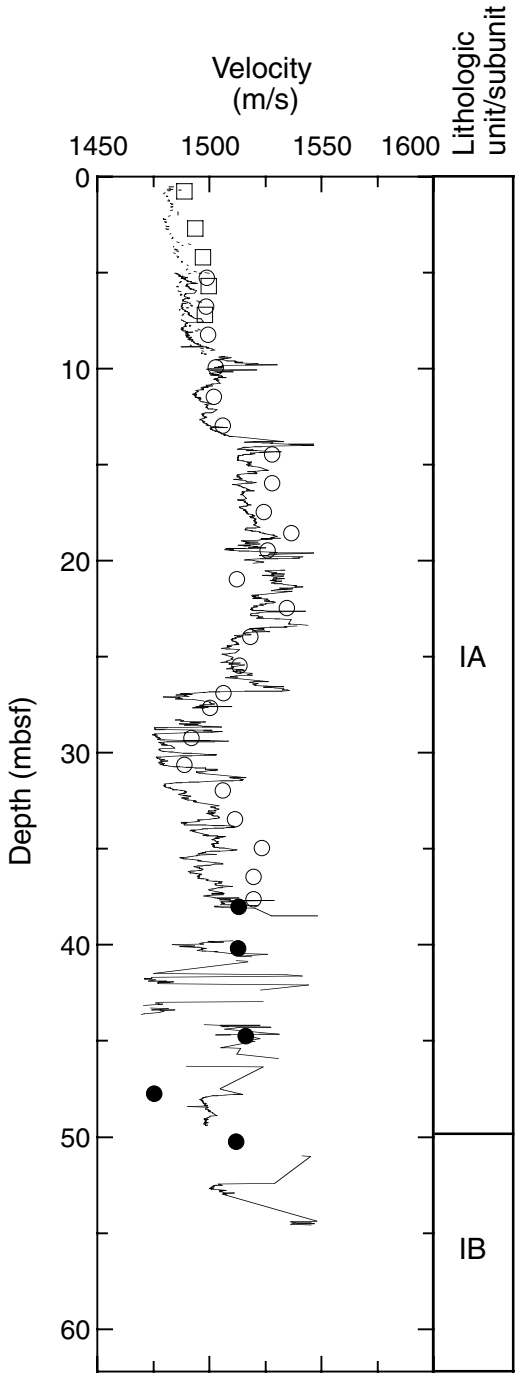

Figure F17. Natural gamma radiation for Holes 1216A (solid line) and 1216B (dashed line). Lithologic Subunits IA and IB are noted on the right side of the figure. cps = counts per second.

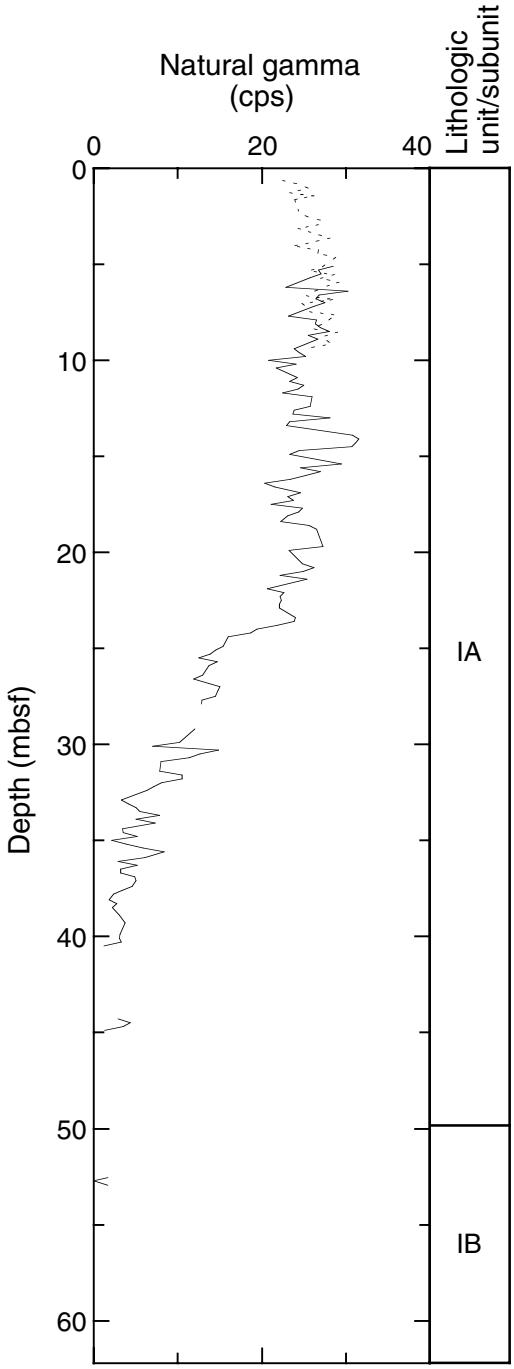

Figure F18. MS for Holes 1216A (solid line) and 1216B (dashed line). Lithologic Subunits IA and IB are noted on the right side of the figure.

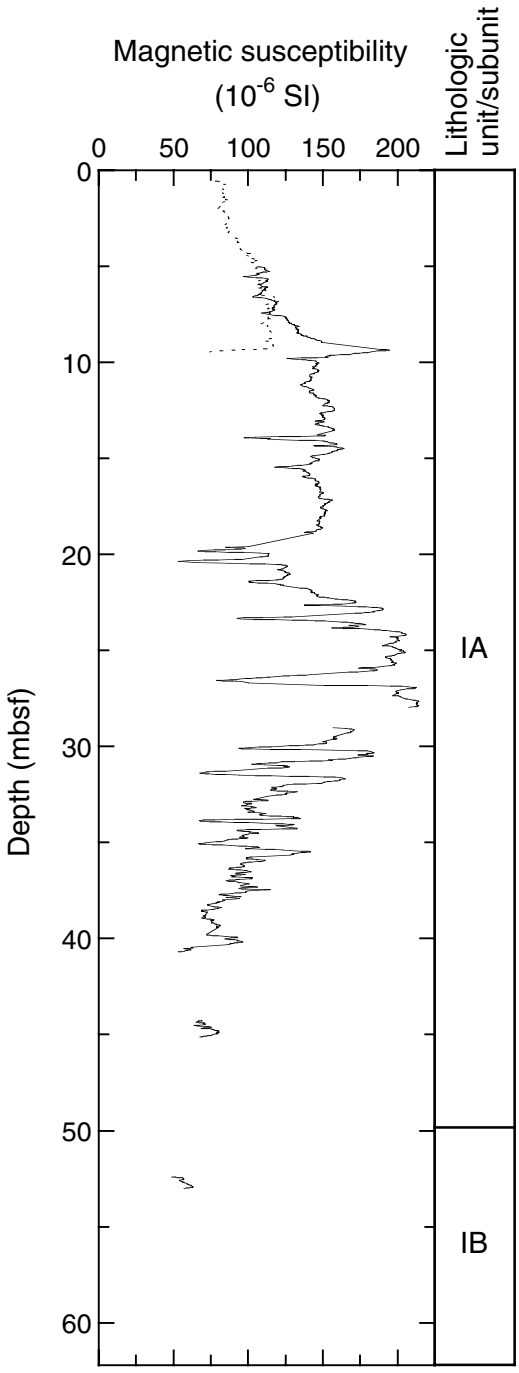

Table T1. Coring summary, Site 1216.

Hole 1216A
Latitude: 21°27.1629′N
Longitude: 139°28.7904′W
Time on site (hr): 42.25 (2130 hr, 5 Nov–1545 hr, 7 Nov 2001)
Time on hole (hr): 31 (2130 hr, 5 Nov–0430 hr, 7 Nov 2001)
Seafloor (drill pipe measurement from rig floor, mbrf): 5163.3
Distance between rig floor and sea level (m): 10.8 m
Water depth (drill pipe measurement from sea level, m): 5152.5
Total depth (drill pipe measurement from rig floor, mbrf): 5225.5
Total penetration (meters below seafloor, mbsf): 62.20
Total length of cored section (m): 62.2
Total core recovered (m): 56.47
Core recovery (%): 90.8
Total number of cores: 11
Total number of drilled intervals: 0

Hole 1216B
Latitude: 21°27.1702′N
Longitude: 139°28.7859′W
Time on hole (hr): 11.25 (0430 hr, 7 Nov–1545 hr, 7 Nov 2001)
Seafloor (drill pipe measurement from rig floor, mbrf) 5158.0 mbrf
Distance between rig floor and sea level (m): 10.8
Water depth (drill pipe measurement from sea level, m): 5147.2
Total depth (drill pipe measurement from rig floor, mbrf): 5167.5
Total length of cored section (m): 9.5
Total length of cored section: 9.5 m
Total core recovered (m): 9.75
Core recovery (%): 102.6
Total number of cores: 1
Total number of drilled intervals: 0

Core	Date (Nov 2001)	Local time (hr)	Depth (mbsf) Top	Depth (mbsf) Bottom	Length (m) Cored	Length (m) Recovered	Recovery (%)
199-1216A-							
1H	6	1440	0.0	9.2	9.2	9.19	99.9
2H	6	1535	9.2	18.7	9.5	9.95	104.7
3H	6	1640	18.7	28.2	9.5	9.40	98.9
4H	6	1745	28.2	37.7	9.5	10.04	105.7
5H	6	1845	37.7	39.7	2.0	1.97	98.5
6H	6	2000	39.7	43.7	4.0	4.06	101.5
7H	6	2115	43.7	46.2	2.5	2.44	97.6
8H	6	2245	46.2	49.8	3.6	3.52	97.8
9H	7	0025	49.8	53.3	3.5	3.47	99.1
10H	7	0200	53.3	54.3	1.0	1.07	107.0
11X	7	0345	54.3	62.2	7.9	1.36	17.2
			Cored totals:		62.2	56.47	90.8
199-1216B-							
1H	7	0615	0.0	9.5	9.5	9.75	102.6
			Cored totals:		9.5	9.75	102.6

Note: The expanded coring summary table is available in ASCII (see the "Supplementary Material" contents list).

Table T2. Distribution of radiolarians, Hole 1216A.

Core, section, interval (cm)	Depth (mbsf)	Preservation	Group abundance	Zone/ Subzone	*Amphicraspedum murrayanum*	*Buryella clinata*	*Calocyclas hispida*	*Calocycloma castum*	*Dictyoprora mongolfieri*	*Eusyringium fistuligerum*	*Eusyringium lagena*	*Lamptonium fabaeforme chaunothorax*	*Lamptonium fabaeforme constrictum*	*Lamptonium fabaeforme fabaeforme*	*Lamptonium sanfilippoae*	*Lithochytris vespertilio*	*Lithocyclia aristotelis*	*Lithocyclia ocellus* gp.	*Lophocyrtis jacchia*	*Lychnocanoma bellum*	*Phormocyrtis striata exquisita*	*Phormocyrtis striata striata*	*Podocyrtis (Lampterium) acalles*	*Podocyrtis (Lampterium) fasciolata*	*Podocyrtis (Lampterium) helenae*	*Podocyrtis (Lampterium) mitra*	*Podocyrtis (Lampterium) sinuosa*	*Podocyrtis (Lampterium) trachodes*	*Podocyrtis (Podocyrtis) papalis*	*Podocyrtis (Podocyrtoges) ampla*	*Podocyrtis (Podocyrtoges) diamesa*	*Podocyrtis (Podocyrtoges) dorus*	*Podocyrtis (Podocyrtoges) phyxis*	*Spongatractus balbis*	*Spongatractus pachystylus*	*Theocotyle conica*	*Theocotyle cryptocephala*	*Theocotyle nigriniae*	*Theocotyle venezuelensis*	*Theocotylissa ficus*	*Thyrsocyrtis (Pentalacorys) tensa*	*Thyrsocyrtis (Pentalocorys) triacantha*	*Thyrsocyrtis (Thyrsocyrtis) hirsuta*	*Thyrsocyrtis (Thyrsocyrtis) rhizodon*	*Thyrsocyrtis (Thyrsocyrtis) robusta*
199-1216A-																																													
5H-CC, 12–17	39.62		B																																										
6H-1, 40–42	40.10	M	R	RP13			X	?	X	X	X					X		X				X				X											X		X					
6H-3, 104–106	43.74	M	F	RP13			X	X	X	X	X					X		X		X						X	X	X		X				X			X		X					
7H-1, 47–49	44.17	P	T	RP12/11					X							X																									X				
7H-2, 47–49	45.67	P	T	RP11			X		X																	X															X	X			
7H-CC, 0–10	46.04	P	R	RP11					X													X				X																			
8H-1, 45–47	46.65	P	R	RP11			X		X							X						X				X													X			X	X		
8H-2, 45–47	48.15	P	R	RP11			X		X							X						X				X						X						X		X	?		X	
8H-3, 45–47	49.25	P	R	RP11			X		X							X													X														X	
8H-CC, 17–22	49.67	P	R	RP11	X			X	X							X						X				X									X		X		X			X	X	
9H-3, 40–42	52.74	R	T	RP11			?	?	X							X										X													X		?			
9H-CC, 10–20	53.17	P	R	RP11			X	X	X							X						X							X			X			X			X		X			
10H-CC, 9–11	54.35		B	RP11																																									
11X-CC, 9–16	55.59	P	T	RP9/10	X	X																							X											X	X				

Notes: Preservation: M = moderate, P = poor. Abundance: F = few, R = rare, T = trace, X = present, B = barren.

Table T3. Distribution of agglutinated benthic foraminifers, Site 1216.

Core, section, interval (cm)	Depth (mbsf)	Preservation	Group abundance	Bathymetry	*Ammodiscus* sp.	*Bathysiphon* spp.	*Trochamminoides proceus*	*Glomospira gordialis*	*Hippocrepinella* sp.	*Miliammina* sp.	*Rhizammina* sp.	*Sorosphaera* sp.	*Subreophax* sp.	*Thalmannammina subturbinata*	*Unidentified benthic forams*	Comments
199-1216A-																
1H-CC, 5–15	9.09	B														
2H-CC, 9–19	19.05	B														
3H-CC, 0–10	28.00	B														
4H-CC, 22–27	38.19	M	A	LA	C	C	R	F		F	R	R	R		C	Tests very brittle
5H-CC, 12–17	39.62	M	A	LA	C	C	R	F		F	R	R	R	F	C	Tests very brittle
6H-3, 104–106	43.74	P	T	LA	C	F									R	Tests very brittle
7H-CC, 0–10	46.04	P	T	LA					C		R			F	R	Tests very brittle
8H-CC, 17–22	49.67	P	C	LA	C		R		C	F	R			F	F	Tests very brittle
9H-CC, 10–20	53.17	P	C	LA	C						R				C	Tests very brittle
10H-CC, 9–11	54.35	B														
11X-CC, 9–16	55.59	B														
199-1216B-																
1H-CC, 10–15	9.70	B														

Notes: Preservation: M = moderate, P = poor. Abundance: A = abundant, C = common, F = few, R = rare, T = trace, B = barren. Bathymetry: LA = lower abyssal.

Table T4. Core disturbance, Site 1216.

Core, section, interval (cm)	Depth (mbsf) Top	Depth (mbsf) Bottom	Comments
199-1216A-			
1H-1, 0–150	0.00	1.50	Disturbed/soupy
1H-2, 0–150	1.50	3.00	Disturbed/soupy
1H-3, 0–147	3.00	4.47	Disturbed/soupy
1H-4, 0–28	4.50	4.78	Disturbed/soupy
1H-4, 28–50	4.78	5.00	Disturbed/soupy
2H-1, 0–10	9.20	9.30	Disturbed/soupy
3H-1, 0–90	18.70	19.60	Disturbed/soupy
3H-2, 0–3	20.20	20.23	Disturbed/soupy
3H-2, 18–22	20.38	20.42	Disturbed/soupy
3H-6, 57–58	26.77	26.78	Disturbed/soupy
3H-6, 50–60	26.70	26.80	Disturbed/soupy
4H-1, 0–82	28.20	29.02	Soupy
4H-1, 112–128	29.32	29.48	Soupy
4H-2, 123–124	30.93	30.94	Soupy
4H-3, 11–12	31.31	31.32	Soupy
5H-1, 0–29	37.70	37.99	Disturbed
5H-2, 40–42	39.10	39.12	Disturbed
6H-1, 0–9	39.70	39.79	Disturbed
6H-1, 64–74	40.34	40.44	Soupy
6H-1, 102–150	40.72	41.20	Soupy
6H-2, 0–150	41.20	42.70	Soupy
6H-3, 0–108	42.70	43.78	Soupy
7H-1, 0–54	43.70	44.24	Chert disturbance
7H-2, 0–65	45.20	45.85	Chert disturbance
7H-2, 65–84	45.85	46.04	Soupy
8H-1, 0–146	46.20	47.66	Flow-in
8H-2, 0–112	47.70	48.82	Flow-in
8H-3, 0–70	48.80	49.50	Flow-in
8H-CC, 0–19	49.50	49.69	Flow-in
9H-1, 0–120	49.80	51.00	Soupy
9H-1, 120–150	51.00	51.30	Chert/downhole debris
9H-2, 0–104	51.30	52.34	Chert/downhole debris
9H-3, 0–6	52.34	52.40	Chert/downhole debris
10H-1, 0–96	53.30	54.26	Chert/downhole debris
10H-CC, 0–8	54.26	54.34	Chert/downhole debris
11X-1, 0–120	54.30	55.50	Chert/downhole debris
11X-CC, 0–10	55.50	55.60	Chert/downhole debris
199-1216B-			
1H-1, 0–45	0.00	0.45	Soupy
1H-2, 0–10	0.45	0.55	Soupy

Notes: Data from these intervals were removed from the GRA bulk density, MS, color reflectance, natural gamma, and *P*-wave velocity data sets presented in this chapter. This table is also available in **ASCII.**

Table T5. Paleomagnetic events, Site 1216.

Chron/ subchron	Age (Ma)	Hole, core, section, interval (cm)	Top (mbsf)	Hole, core, section, interval (cm)	Bottom (mbsf)	Midpoint (mbsf)
		199-		199-		
B C1r.1n	1.07	1216A-2H-1, 80	10.00	1216A-2H-1, 80	10.00	10
B C19n	41.52	1216A-5H-1, 80	38.50	1216A-5H-1, 80	38.50	38.5
T C20n	42.536	1216A-5H-2, 80	39.50	1216A-5H-2, 80	39.50	39.5

Notes: T = top, B = bottom. Paleomagnetic reversals are given as that mcd depth at which the inclination crosses zero (see "Paleomagnetism," p. 7). This table is also available in ASCII.

Table T6. Radiolarian events, Site 1216.

Chron/ subchron	Age (Ma)	Hole, core, section, interval (cm)	Top (mbsf)	Hole, core, section, interval (cm)	Bottom (mbsf)	Midpoint (mbsf)
		199-		199-		
B RP13	44.5	1216A-6H-3, 30	43.70	1216A-7H-1, 49	44.19	43.95
B RP12	47.5	1216A-7H-1, 49	44.19	1216A-7H-2, 49	45.69	44.94
B RP11	48.5	1216A-9H-CC	53.30	1216A-9H-11, CC	55.66	54.48

Notes: B = bottom. Biostratigraphic events are noted with the mcd depth of these samples (see "Biostratigraphy," p. 6). This table is also available in ASCII.

Table T7. Linear sedimentation rates (LSRs), dry bulk density (DBD), and mass accumulation rates (MARs) for major lithologic units, Hole 1216A.

Interval (mbsf)	LSR (m/m.y.)	DBD (g/cm^3)	MAR ($mg/cm^2/k.y.$)
0–4	10.0	0.48	480
4–10	10.0	0.55	550
10–29	0.7	0.55	38
29–33	0.7	0.38	26
33–39	0.7	0.30	21

Notes: Control points for LSR values are shown in Tables **T5,** p. 38, and **T6,** p. 39 p.xx. Sedimentary unit DBD values are compiled from Table **T11,** p. 44. For more information on the major lithologic units see **"Lithostratigraphy,"** p. 4. This table is also available in **ASCII.** [**N1**]

Table T8. Interstitial water data, Hole 1216A.

Core, section, interval (cm)	Depth (mbsf)	pH	Alkalinity (mM)	Salinity	Cl (mM)	Na (mM)	K (mM)	Ca (mM)	Mg (mM)	SO_4 (mM)	NH_4 (μM)	H_4SiO_4 (μM)	Sr (μM)	Li (μM)	Mn (μM)	Ba (μM)	B (μM)
199-1216A-																	
1H-3, 145–150	4.45	7.15	2.48	35.0	560	481	12.7	10.4	52.0	28.4	6.32	210	86	32	1.13	0.21	647.2
2H-3, 145–150	13.65	7.09	2.52	35.0	562	483	12.4	10.0	52.2	27.8	9.44	340	85	32	1.42	0.44	637.4
3H-3, 145–150	23.15	7.11	2.44	35.0	564	484	12.2	9.9	53.1	28.3	6.26	470	84	34	2.76	0.27	591.8
4H-3, 145–150	32.65	7.07	2.49	35.0	564	478	12.0	11.1	55.1	28.2	0.00	606	88	35	2.61	0.29	529.8
8H-3, 145–150*	47.65	7.16	2.74	35.0	559	468	11.7	11.4	58.1	28.6	15.52	708	87	39	1.71	0.54	508.1

Notes: * = sample not displayed in Fig. **F11,** p. 26, because of seawater contamination. This table is also available in **ASCII.**

Table T9. Bulk sediment data, Site 1216.

Core, section, interval (cm)	Depth (mbsf)	Si (wt%)	Al (wt%)	Ti (wt%)	Fe (wt%)	Mn (wt%)	Ca (wt%)	Mg (wt%)	P (wt%)	Sr (ppm)	Ba (ppm)
199-1216A-											
1H-1, 72–73	0.72	25.62	8.50	0.51	5.54	0.91	0.61	2.19	0.12	182.02	1086.98
1H-2, 73–74	2.23	24.92	8.39	0.48	5.40	0.68	0.51	2.01	0.08	172.41	1166.29
1H-3, 74–75	3.74	24.66	8.37	0.47	5.18	0.81	0.69	1.94	0.14	197.98	1195.04
1H-4, 74–75	5.24	24.41	8.11	0.41	4.55	0.97	0.84	1.74	0.20	215.43	566.99
1H-5, 74–75	6.74	23.92	8.05	0.40	4.49	0.88	0.81	1.69	0.20	200.84	538.59
1H-6, 74–75	8.24	23.49	7.77	0.39	4.55	0.93	1.02	1.51	0.24	225.67	506.11
2H-1, 73–74	9.93	23.76	8.34	0.38	4.36	1.07	1.23	1.54	0.33	248.29	661.41
2H-2, 75–76	11.45	23.11	8.04	0.37	4.38	1.14	1.15	1.61	0.25	242.60	710.95
2H-3, 74–75	12.94	23.72	7.87	0.36	4.49	1.09	1.20	1.40	0.23	245.23	564.07
2H-4, 73–74	14.43	23.94	8.29	0.32	4.39	1.45	1.73	1.20	0.48	251.31	430.94
2H-6, 74–75	17.44	23.98	8.17	0.32	4.64	1.43	1.26	1.28	0.25	230.57	447.53
2H-7, 36–37	18.56	22.42	8.02	0.29	4.87	1.57	1.18	1.16	0.28	230.03	517.21
3H-1, 77–78	19.47	23.62	7.69	0.27	5.50	1.96	1.54	1.20	0.43	237.21	449.88
3H-2, 73–75	20.93	22.59	7.70	0.25	4.68	1.56	1.31	1.25	0.30	212.52	407.52
3H-3, 73–75	22.43	22.68	7.44	0.25	6.92	1.58	1.51	1.46	0.39	236.44	553.84
3H-4, 73–75	23.93	22.57	6.97	0.24	8.12	1.61	1.70	1.30	0.44	235.31	408.97
3H-5, 73–75	25.43	21.63	6.26	0.24	9.91	1.90	1.63	1.63	0.42	232.84	486.45
3H-6, 67–68	26.87	19.56	5.80	0.24	12.95	2.10	1.34	1.51	0.34	246.14	411.27
3H-7, 32–33	27.62	21.32	5.94	0.26	16.04	2.72	1.86	1.62	0.43	309.25	693.01
4H-1, 102–103	29.22	17.21	4.28	0.19	17.89	3.76	1.30	1.47	0.28	337.84	913.16
4H-2, 96–97	30.66	17.46	4.50	0.19	16.01	3.51	1.45	1.63	0.37	324.21	723.26
4H-3, 78–79	31.98	18.64	3.75	0.17	12.40	2.33	1.27	1.90	0.29	278.24	1324.44
4H-4, 78–79	33.48	19.93	3.57	0.16	13.49	2.87	1.29	2.11	0.34	303.12	1160.60
4H-5, 78–79	34.98	20.34	3.31	0.14	13.23	3.18	0.94	2.37	0.19	249.09	998.99
4H-6, 78–79	36.48	19.60	3.00	0.15	14.23	3.59	1.22	2.30	0.35	297.31	1499.82
4H-7, 47–48	37.67	18.72	2.45	0.11	12.29	2.75	1.06	2.36	0.27	235.25	1293.26
5H-1, 30–31	38.00	20.37	2.60	0.12	13.03	3.04	1.18	2.31	0.27	268.76	1303.05
5H-2, 59–60	39.29	28.51	1.42	0.07	7.14	1.78	0.36	1.09	0.15	143.29	678.75
6H-1, 46–47	40.16	20.01	2.66	0.13	12.58	3.13	1.24	2.23	0.29	271.78	1937.63
7H-1, 102–103	44.72	20.26	2.84	0.12	11.40	2.89	1.22	2.10	0.39	256.96	1643.72
8H-2, 6–7	47.76	21.23	3.45	0.15	10.37	2.42	1.43	2.46	0.34	258.09	3752.70
9H-3, 45–46	52.79	21.70	2.68	0.09	11.90	3.27	1.20	2.95	0.34	280.67	4237.43
199-1216B-											
1H-2, 73–74	1.18	24.85	8.05	0.47	5.53	1.12	0.66	1.88	0.15	182.14	1275.76
1H-3, 73–74	2.68	24.29	8.24	0.44	5.11	0.78	0.65	1.80	0.16	189.68	1021.67
1H-4, 73–74	4.18	23.83	8.09	0.42	4.87	0.85	0.73	1.74	0.17	201.84	986.61
1H-5, 73–74	5.68	23.09	7.50	0.40	4.64	0.85	0.78	1.59	0.22	198.40	989.02
1H-6, 73–74	7.18	25.30	8.43	0.44	4.96	0.98	0.93	1.76	0.27	234.68	1305.59
1H-7, 73–74	8.68	23.65	7.87	0.40	4.34	0.94	0.87	1.60	0.23	208.38	669.57

Note: This table is also available in **ASCII.** [**N1**]

Table T10. Calcium carbonate ($CaCO_3$) and organic carbon data, Hole 1216A.

Core, section, interval (cm)	Depth (mbsf)	$CaCO_3$ (wt%)	Organic C (wt%)	$CaCO_3$ (wt%)*
199-1216A-				
1H-2, 73–74	2.23	0.15	0.09	–2.92
1H-4, 74–75	5.24	0.38	0.02	–2.05
2H-2, 75–76	11.45	0.21	0.02	–1.22
2H-5, 73–74	15.93	0.27	0.01	
3H-2, 73–75	20.93	0.31	0.00	–0.84
3H-6, 67–68	26.87	0.37	0.00	–0.91
4H-3, 78–79	31.98	1.11	0.00	–1.22
4H-7, 47–48	37.67	0.40	0.00	–1.74
5H-2, 59–60	39.29	0.32	0.00	–3.48
6H-1, 46–47	40.16	0.35	0.00	–1.27
7H-1, 102–103	44.72	0.44	0.00	–1.35
8H-2, 6–7	47.76	0.43	0.00	–0.75
9H-3, 45–46	52.79	0.35	0.00	–1.43

Notes: * = calculated from Ca (in weight percent). $CaCO_3$ calculated from Ca (in weight percent) is not given in some cases because weight percent salt and/or Ca data was unavailable. Negative values may be due to an assumed Ca contribution from aluminosilicates in the normative calculation (see **"Explanatory Notes"** chapter). This table is also available in **ASCII.**

Table T11. Moisture and density measurements, Site 1216.

Core, section, interval (cm)	Depth (mbsf)	Water content (%)	Density (g/cm^3)			Porosity (%)
			Wet bulk	Dry bulk	Grain	
199-1216A-						
1H-1, 75–77	0.75	54.8	1.41	0.64	2.62	75.6
1H-2, 75–77	2.25	54.4	1.41	0.64	2.59	75.1
1H-3, 75–77	3.75	56.3	1.40	0.61	2.66	77.0
1H-4, 75–77	5.25	51.8	1.47	0.71	2.73	74.1
1H-5, 75–77	6.75	52.2	1.44	0.69	2.58	73.3
1H-6, 75–77	8.25	52.9	1.44	0.68	2.66	74.5
2H-1, 75–77	9.95	51.8	1.44	0.69	2.56	72.9
2H-2, 75–77	11.45	52.2	1.44	0.69	2.56	73.2
2H-3, 75–77	12.95	53.8	1.42	0.66	2.60	74.7
2H-4, 75–77	14.45	52.2	1.43	0.68	2.53	73.0
2H-5, 75–77	15.95	54.7	1.40	0.64	2.55	75.0
2H-6, 75–77	17.45	54.6	1.41	0.64	2.56	75.0
2H-7, 37–39	18.57	53.9	1.41	0.65	2.54	74.4
3H-1, 75–77	19.45	60.3	1.34	0.53	2.54	79.0
3H-2, 75–77	20.95	53.9	1.41	0.65	2.50	74.0
3H-3, 75–77	22.45	55.4	1.40	0.62	2.58	75.8
3H-4, 75–77	23.95	55.4	1.42	0.63	2.72	76.7
3H-5, 75–77	25.45	56.4	1.41	0.62	2.74	77.5
3H-6, 69–71	26.89	57.7	1.40	0.59	2.80	78.9
3H-7, 34–36	27.64	57.7	1.40	0.59	2.76	78.6
4H-1, 101–103	29.21	61.2	1.37	0.53	2.94	82.0
4H-2, 93–95	30.63	63.0	1.34	0.49	2.79	82.3
4H-3, 75–77	31.95	65.8	1.29	0.44	2.60	83.0
4H-4, 75–77	33.45	66.4	1.23	0.41	2.07	79.9
4H-5, 75–77	34.95	74.2	1.19	0.31	2.24	86.2
4H-6, 75–77	36.45	69.3	1.21	0.37	2.06	82.0
4H-7, 42–44	37.62	68.0	1.24	0.40	2.22	82.1
5H-1, 32–34	38.02	68.1	1.23	0.39	2.19	82.0
5H-2, 60–62	39.30	63.0	1.32	0.49	2.57	81.1
6H-1, 48–50	40.18	68.1	1.23	0.39	2.17	81.9
7H-1, 104–106	44.74	70.0	1.21	0.36	2.12	82.8
8H-2, 6–8	47.76	66.0	1.25	0.43	2.17	80.4
9H-3, 46–48	52.80	70.6	1.22	0.36	2.24	84.0
199-1216B-						
1H-2, 31–33	0.79	53.8	1.43	0.66	2.66	75.1
1H-3, 75–77	2.70	54.1	1.43	0.66	2.68	75.5
1H-4, 75–77	4.20	54.1	1.43	0.66	2.67	75.4
1H-5, 75–77	5.70	52.5	1.44	0.69	2.65	74.1
1H-6, 75–77	7.20	53.3	1.44	0.67	2.67	74.8

Note: This table is also available in **ASCII.** [**N1**]

Table T12. LAS-based mineralogy, Hole 1216A.

Core, section, interval (cm)	Depth (mbsf)	Calcite (model wt%)	Opal/silica (model wt%)	Smectite (model wt%)	Illite (model wt%)
199-1216A-					
1H-1, 75–77	0.76	15.14	0.00	23.69	61.17
1H-1, 125–127	1.26	2.80	6.52	24.07	66.61
1H-2, 23–25	1.74	9.10	0.99	10.72	79.20
1H-2, 75–77	2.26	9.47	0.85	15.07	74.60
1H-3, 24–26	3.25	0.00	8.42	44.18	47.40
1H-3, 75–77	3.76	10.90	0.00	42.78	46.32
1H-4, 28–30	4.79	0.00	12.06	76.36	11.58
1H-4, 75–77	5.26	13.79	0.00	42.10	44.11
1H-5, 23–25	6.24	0.00	13.04	74.48	12.48
1H-5, 75–77	6.76	8.86	0.59	53.42	37.14
1H-6, 23–25	7.74	0.00	11.17	74.24	14.58
1H-6, 75–77	8.26	5.17	0.00	57.52	37.31
2H-1, 24–26	9.45	0.00	12.83	73.25	13.92
2H-1, 75–77	9.96	11.62	4.37	59.39	24.61
2H-2, 23–25	10.94	0.00	11.85	77.52	10.63
2H-2, 75–77	11.46	19.44	13.76	41.55	25.25
2H-3, 23–25	12.44	6.58	16.24	62.14	15.03
2H-3, 75–77	12.96	25.16	13.26	29.72	31.86
2H-4, 23–25	13.94	22.91	28.58	48.51	0.00
2H-4, 75–77	14.46	26.15	22.57	29.93	21.35
2H-5, 23–25	15.44	13.74	25.13	61.12	0.00
2H-5, 75–77	15.96	19.18	21.52	50.39	8.91
2H-6, 23–25	16.94	17.90	21.01	48.83	12.25
2H-6, 75–77	17.46	25.01	22.14	38.07	14.78
2H-7, 21–23	18.42	22.14	23.82	40.25	13.79
2H-7, 37–39	18.58	25.86	27.76	32.44	13.94
3H-1, 75–77	19.46	24.14	21.14	39.53	15.19
3H-1, 124–126	19.95	16.58	24.39	59.03	0.00
3H-2, 5–7	20.26	13.80	30.81	55.39	0.00
3H-2, 75–77	20.96	20.31	29.63	50.06	0.00
3H-3, 23–25	21.94	13.92	26.34	59.74	0.00
3H-3, 75–77	22.46	22.12	26.68	31.11	20.09
3H-4, 23–25	23.44	7.56	28.99	63.45	0.00
3H-4, 75–77	23.96	20.41	26.24	37.03	16.33
3H-5, 23–25	24.94	4.44	25.99	66.16	3.42
3H-6, 23–25	26.44	0.00	20.44	79.57	0.00
3H-7, 23–25	27.54	5.80	24.65	65.32	4.23
4H-2, 24–26	29.95	13.65	6.38	79.97	0.00
4H-3, 24–26	31.45	3.17	9.81	87.02	0.00
4H-3, 75–77	31.96	5.37	14.42	80.21	0.00
4H-4, 24–26	32.95	0.00	25.13	74.87	0.00
4H-4, 75–77	33.46	0.00	19.47	80.53	0.00
4H-5, 24–26	34.45	0.00	20.21	79.79	0.00
4H-5, 75–77	34.96	0.00	15.78	84.22	0.00
4H-6, 24–26	35.95	0.00	15.35	84.65	0.00
4H-6, 75–77	36.46	0.00	10.35	89.65	0.00
4H-7, 24–26	37.45	0.00	21.04	78.96	0.00
4H-7, 42–44	37.63	0.00	15.78	84.22	0.00
5H-1, 32–34	38.03	0.00	12.22	87.78	0.00
6H-1, 22–25	39.93	0.00	20.13	79.87	0.00
6H-1, 48–50	40.19	0.00	7.13	92.87	0.00
7H-1, 104–108	44.76	0.00	14.41	85.59	0.00
7H-2, 23–25	45.44	0.00	5.16	94.84	0.00
8H-1, 126–128	47.47	0.00	20.95	79.05	0.00
8H-2, 6–8	47.77	0.00	19.55	80.45	0.00
8H-2, 23–25	47.94	0.00	22.56	77.44	0.00
8H-3, 23–25	49.04	0.00	20.36	79.64	0.00
9H-3, 23–25	52.58	0.00	21.92	78.08	0.00
9H-3, 46–48	52.81	0.00	18.90	81.10	0.00

Note: This table is also available in **ASCII.** [**N1**]

Table T13. Split-core velocity measurements, Site 1216.

Core, section, interval (cm)	Depth (mbsf)	Velocity (m/s)			Anisotropy (%)
		z*	y*	x†	
199-1216A-					
1H-4, 76	5.26	1484	1499		1.0
1H-5, 76	6.76	1484	1499		1.0
1H-6, 76	8.26	1485	1500		1.0
2H-1, 76	9.96	1492	1503		0.8
2H-2, 76	11.46	1490	1502		0.8
2H-3, 76	12.96	1498	1506		0.5
2H-4, 76	14.46	1513	1528		1.0
2H-5, 76	15.96	1521	1528		0.4
2H-6, 76	17.46	1511	1524		0.9
2H-7, 38	18.58	1521	1537		1.0
3H-1, 76	19.46	1510	1526		1.0
3H-2, 76	20.96	1524	1512		–0.7
3H-3, 76	22.46	1516	1535		1.3
3H-4, 76	23.96	1509	1518		0.6
3H-5, 76	25.46	1505	1514		0.5
3H-6, 70	26.90	1489	1506		1.2
3H-7, 35	27.65	1483	1500		1.2
4H-1, 101	29.21	1474	1492		1.2
4H-2, 93	30.63	1494	1489		–0.3
4H-3, 76	31.96	1489	1506		1.1
4H-4, 76	33.46	1493	1512		1.3
4H-5, 76	34.96	1515	1524		0.6
4H-6, 76	36.46	1494	1520		1.7
4H-7, 43	37.63	1493	1520		1.8
5H-1, 34	38.04			1513	
6H-1, 49	40.19			1513	
7H-1, 105	44.75			1516	
8H-2, 7	47.77			1476	
9H-3, 47	52.81			1512	
199-1216B-					
1H-2, 32	0.77	1478	1489		0.8
1H-3, 76	2.71	1479	1494		1.0
1H-4, 76	4.21	1482	1497		1.0
1H-5, 76	5.71	1487	1500		0.9
1H-6, 76	7.21	1487	1498		0.7

Notes: * = determined by insertion probe, † = determined by contact probe. This table is also available in **ASCII.**

Table T14. Thermal conductivity, Site 1216.

Core, section, interval (cm)	Depth (mbsf)	Thermal conductivity (W/[m·K])
199-1216A-		
1H-3, 76	3.76	0.79
2H-3, 76	12.96	0.81
3H-3, 76	22.46	0.75
4H-3, 76	31.96	0.73
8H-3, 41	49.21	0.75
9H-3, 30	52.64	0.69
199-1216B-		
1H-3, 76	2.71	0.87

Note: This table is also available in **ASCII.**

CHAPTER NOTE

N1. 13 December 2002—After the CD-ROM version of this volume was published, errors were noted in the ASCII versions of Tables T7, T9, T11, and T12. This version contains the corrected ASCII files.

*Dates reflect file corrections or revisions.